

Fermi National Accelerator Laboratory

FERMILAB-Pub-87/171-E

[E-741/CDF]

## An Electromagnetic Calorimeter for the Small Angle Regions of the Collider Detector at Fermilab\*

G. Brandenburg, D. Brown, R. Carey, M. Eaton, A. Feldman, E. Kearns,  
J. Oliver, E. Sadowski, R. Schwitters, M. Shapiro, and R. St. Denis  
*Harvard University, Cambridge, MA 02138*

J. Bensinger, C. Blocker, M. Contreras, L. Demortier, P. Kesten,  
L. Kirsch, H. Piekarz, L. Spencer, and S. Tarem  
*Brandeis University, Waltham, MA 02254*

July-August 1987

\*Submitted to Nucl. Instrum. Methods A



Operated by Universities Research Association Inc. under contract with the United States Department of Energy

## An Electromagnetic Calorimeter for the Small Angle Regions of the Collider Detector at Fermilab

G. Brandenburg, D. Brown, R. Carey, M. Eaton, A. Feldman, E. Kearns,  
J. Oliver, E. Sadowski, R. Schwitters, M. Shapiro, R. St. Denis  
*Harvard University, Cambridge, MA 02138*

J. Bensinger, C. Blocker, M. Contreras, L. Demortier, P. Kesten,  
L. Kirsch, H. Piekarz, L. Spencer, S. Tarem  
*Brandeis University, Waltham, MA 02254*

Two large electromagnetic calorimeters have been built for the Collider Detector at Fermilab (CDF). These have been designed for use in the small angle regions in both the proton and the anti-proton beam directions. Each calorimeter consists of 30 sampling layers of proportional tube chambers with cathode pad readout separated by lead sheets for a total thickness of 25.5 radiation lengths. Each proportional tube chamber is constructed using a novel technique in which the insulating side of the cathode pad board is bonded to the proportional tube walls using resistive epoxy. The measured energy response of the calorimeter is linear up to 160 GeV, and the measured energy resolution,  $\sigma_E/E$ , is approximately  $25\%/\sqrt{E} + 0.5\%$ . The position resolution for single electrons varies between 1 and 4 mm depending on location in the calorimeter. The calorimeter offers good  $e/\pi$  discrimination, where typically the pion misidentification probability  $f_{\pi \rightarrow e} < 0.5\%$  for an electron identification efficiency  $\epsilon > 90\%$ .

# 1 Introduction

With the advent of high energy colliding beam accelerators, calorimetry has become an important tool for the measurement of energy flow in events. A calorimeter is capable of measuring not only the energy of the charged particles but that of the neutrals as well. Unlike a tracking chamber, a calorimeter with tower geometry does not suffer ambiguities in a high multiplicity environment and it can provide simple signatures for interesting events to the trigger electronics. A further benefit is that the energy resolution of a calorimeter improves as the energy deposition increases. An isolated high energy electron is an example of an important physics signature for which a calorimeter is particularly well suited.

The Collider Detector at Fermilab[1] (CDF) has electromagnetic and hadronic calorimetry which cover the polar angle from  $2^\circ$  to  $178^\circ$  with respect to the beam direction and the full azimuthal angle. This coverage is accomplished by dividing the calorimetry into several systems which use different detector techniques. All of these systems use a tower geometry to measure the energy flow in uniform bins of azimuthal angle and pseudorapidity. This article discusses the design and testing of the CDF Forward Electromagnetic Calorimeter system which covers the polar angle region  $2^\circ$  to  $10^\circ$  at both ends of the detector.

The Forward Electromagnetic Calorimeter (FEMC) is segmented into bins of constant azimuthal angle and pseudorapidity to match the overall granularity of CDF. The distance from the collision point was chosen such that the smallest bins are matched to the size of an electromagnetic shower. Given the need for flexibility in the choice of detector element geometry in this region and the need for a radiation resistant design, proportional tube chambers with cathode pad readout were chosen for the sampling medium and lead sheets for the radiator. A sturdy chamber design was sought which would cover a large area (approximately  $2 \text{ m}^2$ ), yet would facilitate chamber repair and replacement when required. The resulting detector is capable of measuring the electromagnetic energy flow with high precision and its granularity provides excellent position resolution.

The following section presents the technical details of this calorimeter design. Following that there is a description of the production and quality control testing of the chambers. The readout electronics, gas system and gain monitoring are then described. This article concludes with results from test beam studies of the calorimeter.

## 2 Technical Description

One end of the CDF detector is shown schematically in figure 1. The Forward Electromagnetic Calorimeters are located approximately 6.5 m from the interaction point and enclose the beam pipe at either end of CDF. Each calorimeter consists of 30 sampling layers, each of which is composed of a lead sheet and a chamber of gas proportional tubes with cathode pad readout. The lead sheets are 80% of a radiation length thick and contain 6% antimony for improved strength and flatness. The gas tubes are run at a nominal high voltage of

1900 volts, which is in the middle of the proportional region. Figure 2 shows a perspective view of one half of one calorimeter. Each calorimeter is roughly 3 m on a side, 1 m deep, and weighs about 18 metric tons.

The proportional tube layers in the calorimeter are divided into quadrants, each of which is a self-contained chamber which can be removed if repairs are required. The cathode pad geometry of a typical chamber is shown in figure 3. Each pad subtends 0.1 units of pseudorapidity  $\eta$ , where  $\eta \equiv -\ln \tan \theta/2$ , and five degrees of azimuthal angle  $\phi$ . The pads are ganged longitudinally into towers with two depth segmentations, both of which are 15 layers thick. The cathode pads are scaled in size every other layer so that the resultant towers project back to the nominal beam-beam interaction point. There are 1440 pads per layer, resulting in a total of 5760 tower segments to be read out for both ends. The anode wires are strung vertically and are ganged together in five sectors per chamber. These sectors are read out independently for each layer, resulting in an additional 150 signals per quadrant. The anode information is intended primarily for diagnostic purposes, but also provides a longitudinal profile of the energy deposition for each sector.

One side of each chamber in the calorimeter consists of an aluminum channel plate which forms three walls of the 124 proportional tubes. A cross sectional view of a chamber is shown in figure 4. Each tube has an inner cross section of 7 mm in the beam direction and 10 mm transverse to the beam. The tubes are separated from each other by a 1.6 mm aluminum wall. The channel plate is manufactured by attaching extruded aluminum channels having a "T" profile to a large aluminum sheet with conductive epoxy. After extruded plastic electrode strips are epoxied to both ends of the channel plate, a 50 micron gold-plated tungsten wire with nickel flashing[2] is strung in each of the tubes. The wires are soldered to electrodes embedded in the plastic strips as shown in figures 6 and 7. The nickel flashing is required to obtain a reliable solder connection. With this geometry and a gas mixture of equal parts of argon and ethane, a nominal gas gain value of 5000 is obtained at the operating high voltage, 1900 volts. A cutaway view of a chamber and details of its construction are shown in figures 5, 6 and 7 respectively.

The cathode pad geometry for each chamber is etched on three fiberglass (FR4) panels, each of which is copper-clad on one side. The fiberglass side of the cathode pad panels is then directly bonded to the aluminum channel plates with resistive epoxy, which forms both the mechanical bond and serves as a resistive path to ground for positive ions resulting from electron avalanches. The epoxy is silk-screened onto the fiberglass surface, resulting in a very uniform coating approximately 75 microns thick. The epoxy mixture can be adjusted at preparation so that the resulting surface resistivity after curing is between 20 and 80 M $\Omega$  per square. The base mixture used is Abatron 8302 [3], which yields a surface resistivity of approximately 1 M $\Omega$  per square. A 40% admixture of an insulating epoxy, Abatron 50, then yields the desired resistivity. The chamber performance is not sensitive to variations in the surface resistivity in this range. For higher surface resistivities, high rate environments will cause positive ions to build up on the resistive surface, resulting in a local decrease in the gain of the chamber. For lower values of the surface resistivity, the induced

charge distribution will be dissipated too quickly as the resistive surface restores itself to ground potential. If the charge integration time in the front end electronics is of the order of the time for the resistive surface to return to ground potential, part of the induced charge will be lost. This effect can be seen graphically in the effective chamber circuit diagram shown in figure 8. The resistive epoxy forms an effective RC shunt to ground for the cathode signal with "R" given by the surface resistivity and "C" approximately equal to one picofarad.

Cathode signals are carried to the edge of the chamber by a ribbon cable harness. These ribbon cables are run in the cavity between the cathode pad panels and the outside aluminum wall of the chamber. The signal wires in the ribbon cables are soldered directly to the pad surface, while the ground wires are grounded at the chamber edge and are left unconnected at the pad end. The ends of the signal wires at the chamber edge are series terminated in a  $100\ \Omega$  resistors as shown in figures 6 and 8. These resistors reduce "ringing" of signals between longitudinally ganged pads. The resistors are mounted on a circuit board transition strip which takes the signals through the gas seal to external edge connectors.

A completed chamber is an aluminum box about 1.5 m on a side and about 1.6 cm thick. Extending from the box on one exterior edge are the ribbon cable edge connectors for the 360 cathode pad signals and the 5 sector anode signals, a single high-voltage connector, and the gas inlet and outlet. The other exterior edge has a plastic rail for supporting the chamber in the final mounting frame. On the corner of the two interior edges there is a three-sided notch which forms the octagonal beam hole in the final calorimeter.

The hadron calorimeter for the same angular region in CDF is constructed using chambers with essentially the same design as those described here[4]. It consists of 20 layers of chambers separated by 5 cm thick iron plates, and is completely shadowed by the FEMC. The "Endplug" angular region, from  $10^\circ$  to  $30^\circ$  in polar angle, contains gas-tube calorimeters of similar design[5,6]; however, the tubes are constructed using resistive plastic instead of aluminum and fiberglass.

### 3 Production and Testing

FEMC chambers are constructed in a multi-stage assembly line at the Harvard University High Energy Physics Laboratory (HEPL). Each chamber spends one day at each of several assembly tables. The table tops are very flat aluminum plates which minimize mechanical distortions in the chambers. At the first table, the aluminum T's are epoxied onto an aluminum sheet to form the channel plate. An inflatable bag keeps the assembly flat while the epoxy cures.

At the second and third tables plastic electrode strips are epoxied to the channel plate and anode wires are soldered to the strips. Care is taken in handling the wires as kinks can result in discharges or in excessive current draw. The three cathode pad panels are applied at the fourth table. First resistive epoxy is applied to the panels with a 75 micron

mesh silk screen. The panels are then secured in place until the epoxy cures by a rubber blanket which is held down by a vacuum system. Since the resistivity of the resistive epoxy is a sensitive function of the ambient temperature, the exact proportions of the epoxy ingredients and the standing time of the mixture before application, these variables need to be carefully controlled.

At the the fifth table, the chamber side pieces are epoxied in place. These pieces are fitted carefully to prevent gas leaks which will compromise the performance of the chamber. In the next steps the readout cables and the high voltage leads are soldered in place, and the aluminum top is epoxied on. Again, care is taken to prevent gas leaks. Finally the resistors, capacitors, high voltage connector, ground straps, and hanging bar are attached.

There are five performance tests made during chamber construction. A high voltage test is made at three stages: after the anode wires are strung, after the cathode pad panels are applied, and just before the aluminum cover is epoxied. During the check, the voltage on each of the five high voltage regions is brought to 3.2 kV. Each region is checked for sparks, loose wires and wires which display discharge. In the second test, the resistivity of the epoxy on the three installed cathode pad panels is measured. A square wave is applied to the anode wires and the induced charge on the cathode pads is measured with a charge-integrating amplifier. The time for the charge to decay to  $1/e$  of its original value is measured on an oscilloscope. Since this decay time is proportional to the surface resistivity, this is a direct measurement of the resistivity of the cured epoxy. The third test is a continuity test for the cathode signals, which ensures a good connection between the pads and the pins on the edge connectors. The fourth test comes when the chamber is fully assembled. The chamber is filled with argon-ethane and the seams are checked for leaks with a flammable gas detector; any leaks are filled with epoxy.

The fifth test is performed just before each chamber is shipped to Fermilab. The chamber is irradiated with a  $^{106}\text{Ru}$  beta source for 4-5 minutes at various points over its active surface. A spectrum of the integrated charge from the appropriate cathode pads is accumulated. The resulting charge distribution above a certain threshold is empirically found to have an exponential behavior, as is shown by a typical spectrum in figure 9. The exponential coefficient is inversely proportional to the chamber high voltage as illustrated in figure 10. Therefore with fixed high voltage any variations in the coefficient correspond to chamber gain variations of the opposite sign. For a typical chamber the observed variation is of order 7%. Variations of this size are intrinsic to this method of testing and are not necessarily related to the chamber being tested. The results of this test are not used as a calibration but merely as a final diagnostic tool of the health of the chamber.

Before assembling the chambers into the final calorimeter at Fermilab, the chambers are again tested for high voltage integrity, internal electrical problems and gas leaks. To test for internal electrical problems, the anode wires of the chamber are pulsed and the induced charge is measured from the cathode pads. Figure 11 shows the response of a typical chamber to wire pulsing. The proportionality constant between signal and pad area is a measure of the pad capacitance and agrees with a calculation using the known chamber geometry. To test the chambers for gas leaks, the chambers are pressurized and

the pressure decay-time is measured. The maximum allowed decay rate is 10%/hour. It is estimated that this will keep the air contamination level in a chamber below 1% under normal operating conditions.

## 4 Readout Electronics

The cathode pads that make up a tower are passively added together with a  $100\ \Omega$  resistor in series with each pad (see figure 8). Each tower segment is then connected by approximately 3 meters of ribbon cable to a low noise charge integrator, whose output is connected to sample-and-hold circuits. There are 24 channels of integrators and associated sample-and-holds packaged on a board which is designed to fit into a RABBIT system[7] crate. In addition to the boards of charge integrators and sample-and-holds, each RABBIT crate contains two 16-bit ADC's. The output of the sample-and-holds are sequentially multiplexed to one of the ADC's, the voltage digitized, and the result sent to the CDF data acquisition system[8].

The sample-and-holds are a novel measurement scheme designed for a high rate environment. There are two sample-and-hold circuits on each integrator, one of which ("before") samples the output just before beam crossing and one of which ("after") samples the output after the charge from the event has been integrated. The integration time is about  $1.5\ \mu\text{sec}$  for this calorimeter. The ADC in the RABBIT system digitizes the difference between the output of the "after" sample-and-hold and the output of the "before" sample-and-hold, giving a result proportional to the charge integrated in that event. The integrators have a passive reset with a  $100\ \mu\text{sec}$  time constant. The amplifier gains of the charge integrators are set so that full scale corresponds to an energy of 400 GeV. Thus, on the 16-bit ADC of the RABBIT system, the least count is 6 MeV. The gains are very stable, typically having a temperature coefficient of 0.02% per degree C, with a maximum nonlinearity of 0.15% of full scale.

The inherent pedestal widths due to electronic noise are 2 to 5 counts, depending on the source capacitance of the tower. The pedestal values are also quite stable, having temperature coefficients of less than 1 count per degree C. In addition to the charge integrator and sample-and-hold circuits, each board of 24 channels has a single, precision charge injection system which is multiplexed to the inputs of the integrators for calibration. The injected charge has an absolute accuracy of 0.5% .

High voltage is distributed to the anode wires using a system developed for CDF[9]. CAMAC controlled bulk supplies are located in the CDF counting room and feed distribution cards which are located in RABBIT crates in the collision hall. The HV distribution cards have twenty channels which provide high voltage to individual chambers. Each channel has its current monitored and is controlled by a high voltage relay. The status of the high voltage system is continuously monitored by the CDF alarms and limits system.

The anode wires from each high voltage region are connected to a charge integrator on a RABBIT card (32 channels per card) via a 10 nF high-voltage blocking capacitor. The

anode readout cards use a before-after sample-and-hold scheme similar to the pad readout. The anode information is primarily used for monitoring chamber performance. However, for isolated showers, the longitudinal shower profile obtained from the anode data is useful for electron-pion separation.

## 5 Gas System

The forward electromagnetic calorimeter uses argon-ethane 50–50 for its gas mixture as do the other gas calorimeters in the CDF detector. A small admixture of isopropanol may be used to prevent glow discharges[10]. Ethanol, which is used by other calorimeters for this purpose, has a deleterious effect on the resistive epoxy used in the chamber construction and cannot be used. The nominal gas flow is one volume every two days (1200 liters per day per calorimeter) with a purge flow of five times that rate. A major constraint on the gas system is posed by the large surface area of the gas volume of each chamber: substantial pressure differentials could damage chambers. To minimize the forces on the aluminum tops, the gas control system is designed to maintain the gas pressure within 1 mm of water of atmospheric pressure.

Figure 5 shows a cutaway view of a chamber. Gas flow in the chamber is parallel through each tube. The tubes are fed through the cavity above the high voltage bus, and exhaust through the cavity above the anode wire electrodes at the other end. It is important to keep the flow impedance nearly equal for all tubes, as a few percent difference in impedance would result in uneven gas flow and possible gain variations.

The gas control system is a double-buffered, symmetric pressure design. A block diagram of the system is shown in figure 12. Two hundred liter input and exhaust buffers, which operate equally above and below atmospheric pressure (typically 5 mm of water), isolate the calorimeter from the CDF central gas supply. These buffer tanks drive the input and exhaust lines for each of the quadrant manifolds. The gas lines from the manifolds to the individual chambers have an impedance 100 times greater than that of the chambers, thus the flow to each chamber is essentially the same independent of impedance variation between chambers. Flow to and from the quadrant is regulated by solenoid valves controlled by pressure gauges. Typically the pressure in the manifolds is maintained within 1 mm water of atmospheric. The CDF alarm system generates an alarm if any manifold has a pressure of more than 2 mm of water beyond its set point. The input (exhaust) manifolds and buffers both have safety vents which prevent any substantial over (under) pressure. As an additional safety, solenoid valves are placed so that in the event of a major power failure the gas system is closed to the main CDF gas supply. This system also supplies gas for the forward hadron calorimeters.

## 6 Source Monitoring

The gas gain of a proportional chamber, and hence the energy calibration of a gas-sampling calorimeter, is a sensitive function of temperature, pressure, high voltage, gas composition, wire diameter, and wire position, with the relative change in the gas gain being roughly an order of magnitude larger than the relative change in any of these variables[11]. Wire diameter and wire position affect spatial uniformity, whereas the other four quantities contribute to temporal variations of the calorimeter response.

The pressure, temperature, and gas composition are difficult to control to the accuracy required. For this reason, the gas gain of the calorimeter is monitored continuously by radioactive sources. There are two types of monitors; embedded sources and gas-monitor tubes. Both monitors use  $^{55}\text{Fe}$  as their radioactive source. The two embedded sources per quadrant are placed on dedicated pads inside a chamber near shower maximum. One of these is outside the  $10^\circ$  radius and the other is inside the  $2^\circ$  radius. The sources allow both overall gain shifts of the calorimeter and potential gain differences within the chamber to be monitored. In addition, there are two gas-monitor tubes per quadrant consisting of cylindrical proportional tubes using the same wire and having roughly the same cross-sectional area as a tube in the calorimeter chambers. Pressure and temperature transducers on each of the monitor tubes allow direct measurements of two of the four temporal variables affecting gas gain. The argon-ethane mixture is delivered to the CDF central gas handling facility by a vendor. The mixture is then checked by measuring the gas gain in a monitor tube. If necessary, additional argon or ethane is added to bring the gain to a predetermined point before it is distributed to the calorimeters.

The signals from both monitor tubes and embedded sources are processed separately from the event data stream. Source signals are sent to special charge integrating amplifier cards in a RABBIT crate near the calorimeters. The amplifier output channels are tapped for the monitor tube trigger which in turn generates a microprocessor interrupt. The microprocessor commands the RABBIT system to digitize the channel that caused the trigger, and then reads out and stores the data. Spectra are accumulated in this manner for all the source monitors in the system and are fitted for the position and width of the peak from the 5.9 keV  $^{55}\text{Fe}$  line. A complete set of source results are uploaded to the alarms and limits computer every half hour. Source monitoring results are saved for further analysis and are also used to correct the calorimetry trigger constants.

The ability of the gas-monitor tubes to track the gas gain of the calorimeter was studied during the beam test of the calorimeter. The tubes used the same gas mixture as the calorimeter and were placed in very close proximity to the chambers to minimize pressure and temperature differentials. In addition, the monitor tubes were run from the same high voltage supply as the chambers. The result is shown in figure 13, where the peak position resulting from the 5.9 keV X-ray from a  $^{55}\text{Fe}$  source is plotted against the mean energy deposition from 100 GeV electrons for several different runs at different locations on the calorimeter. Over a period of weeks it was found that the gas monitor tubes and the calorimeter gain tracked to within 2%.

## 7 Beam Test

An extensive program of testing and calibration of the calorimeter was undertaken at the M-Bottom beam line at Fermilab. From January to June of 1985 four completed quadrants were tested. The M-Bottom beam line provided secondary electrons and pions from the debris of an 800 GeV proton beam incident on a fixed target. The secondary beam particles were available in a range of momenta from 20 to 200 GeV, with a momentum spread of roughly 5% around the central value. Momentum measurement and beam position tagging were accomplished by multiwire proportional wire chambers located at each end of a dogleg bend. The trigger was configured with scintillator paddles at each end of the bending magnets, including a halo veto. The read-out electronics were a version of the RABBIT system[7] which utilized a special CAMAC interface to read the digitized signals. For the beam test, a calorimeter quadrant was suspended by a special rig designed to move the calorimeter around the fixed beam axis in such a way as to align the projective tower geometry of the calorimeter with the incident beam. This is shown in figure 14.

Figure 15 shows the distribution of charge measured from a sample of 100 GeV electrons. Each channel (tower) is corrected for amplifier gain and pedestal. The total charge is measured by finding the tower with the highest energy and summing that value with all surrounding towers that are above pedestal. Further towers are added if they are above pedestal and are adjacent to a tower already included in the energy cluster. The total charge is renormalized to the central beam momentum using the value for the momentum measured by the beam PWC's. The resulting distribution is fit to a gaussian; the mean is used to study the response of the calorimeter and the width is used to study its resolution.

The response of the calorimeter to electrons of various energies at a fixed location is shown in figure 16. The data from 20 to 120 GeV are fit by a straight line with slope  $1.90 \pm 0.01$  pC/GeV and intercept  $1.83 \pm 0.04$  pC. Some leakage or saturation is indicated at higher electron energies. The energy resolution, as seen in figure 17, is approximately 3% at 100 GeV, and varies as  $1/\sqrt{E}$  as expected for a sampling calorimeter. A fit to the data gives an energy resolution of  $\sigma_E/E = (25.4 \pm 0.7)\%/\sqrt{E} + (0.47 \pm 0.01)\%$ .

The response of the calorimeter to 100 GeV electrons at a fixed location is shown in figure 18 as a function of high voltage. The high voltage dependence is exponential in the vicinity of the nominal operating point of 1900 volts. A fit to the data of the form  $ae^{-bV}$  gives  $b = 0.0095 \pm .0004$   $V^{-1}$ . This corresponds to a doubling of the gain approximately every 75 volts.

The response of the calorimeter was measured as a function of position over the face of the calorimeter. A sample of 100 GeV electrons was taken at the center of each trigger cluster, where a trigger cluster is a group of six pads 0.2 units in  $\eta$  by 15 degrees in  $\phi$ . After cutting on total calorimetric energy and removing showers with poorly measured beam momentum, a gaussian fit was made to the peak in the energy distribution. The monitor tube data was used to correct the data on a run by run basis, and the resulting calorimeter response is plotted separately as a function of  $\eta$  and  $\phi$  in figure 19. In this plot, the data points plotted versus  $\eta$  have been averaged over  $\phi$ , and the data points plotted

versus  $\phi$  have been averaged over  $\eta$ . The data are from three separate quadrants; one of the three has two independent measurements displayed.

The response in the center of the calorimeter is flat with a deviation of less than 5% between quadrants. Energy leakage is apparent at the inner pads (large  $\eta$ ) and possibly at the outermost guard ring. However, the response in  $\phi$  shows anomalously high gain near the vertical edge of the calorimeter. This is probably correlated with rotating the calorimeter test rig to an extreme angle. The rotation is only necessary to align the pad towers with the test beam; the calorimeter will remain upright during actual running. This effect will be re-examined by exploiting the azimuthal symmetry of energy flow in the colliding beam environment.

Alignment of the tower structure with the test beam direction allowed the position resolution of electron showers to be studied. Because the pad sizes are of the same order as the shower size, it is possible to improve on the measurement of the shower center as given by a simple centroid by exploiting the distribution of charge in the various pads. The electron position is found by fitting the transverse profile of each shower to a parameterization. This method is independent of both the location within the calorimeter and the size of the pads, and has only a weak energy dependence.

Figure 20 shows the integral of the transverse shower profile in one coordinate at 100 GeV. The horizontal axis is the distance from the electron impact point to a global calorimeter boundary (here,  $\phi = 15^\circ$ ); the vertical axis is the fraction of the total charge in towers to a given side of that boundary. The function which is fitted to these points is then a measure of the transverse shower profile. This function can be inverted to find the electron position relative to the boundary. An absolute position is found by adding in the known boundary position, and taking a weighted average of the fit values for all the boundaries crossed by a shower.

Figure 21 shows the electron position measured in this manner for a series of data taken at various radii at a constant azimuthal angle. The small hook at the lower end is the result of leakage at the inner edge of the calorimeter. Slices of this plot perpendicular to the diagonal were made to find the spatial resolution. Figure 22 shows the mean and sigma of gaussian fits taken at different points along the position scan in figure 21. The position resolution (sigma) is approximately constant at 1.2 mm near tower boundaries, and varies from 1.3 mm to 3.9 mm at tower centers, increasing with tower size. The absolute position (mean) is within one standard deviation of that measured by the beam PWC's.

The dependence of transverse shower shape and position resolution on the electron energy was studied for a medium-sized pad. The parameters of the fits to the transverse profile have a slight energy dependence. Figure 23 shows the position resolution as a function of energy using the measured energy dependence of these parameters. The approximate  $1/\sqrt{E}$  dependence of the position resolution is consistent with that expected from shower statistics.

The M-Bottom test beam also provided pions from 20 to 200 GeV making preliminary studies of electron/pion discrimination possible. The  $e/\pi$  discrimination in the forward region of CDF is based on the detailed analysis of the particle's energy deposition in the

forward calorimetry in the absence of a momentum measurement. Four variables are used for  $e/\pi$  discrimination; the energy deposited in the front section of the electromagnetic calorimeter,  $E_f$ , the energy deposited in the electromagnetic calorimeter,  $E_{em}$ , the energy deposited in the hadron calorimeter,  $E_{had}$ , and the transverse shower width,  $W$ . As there was no hadron calorimeter available for the beam test, the following analysis utilizes the measured beam momentum,  $p$ , from the PWC's rather than the total calorimetric energy measurement,  $E = E_{em} + E_{had}$ . These variables are combined to provide particle identification based on the different characteristics of electron and pion showers. The electron efficiencies,  $\epsilon$ , and the pion misidentification probabilities,  $f_{\pi \rightarrow e}$ , for the  $e/\pi$  discrimination criteria described below are shown in table 1.

Electron identification is based primarily on the fact that electrons shower early in the calorimeter. Since the calorimeter is approximately one interaction length deep, a typical hadron has a 50% probability of interacting with the interactions uniformly distributed over the depth of the detector. Usually a substantial fraction of the hadron's energy will escape out the back of the detector. Therefore electrons can be identified by the requirement that little energy be present in the hadron calorimeter. Figure 24 shows the distribution of electromagnetic energy for 60 GeV electrons and pions expressed in picocoulombs. For momentum tagging resolution of 0.5%, the cut labeled as **A** corresponding to  $E_{em}/p > 0.89$  accepts 95% of the electrons while misidentifying roughly 2% of the pions.

The pion misidentification probability can be further reduced by exploiting the large fluctuations in hadron shower development for pions depositing most of their energy in the electromagnetic calorimeter. Figures 25 and 26 show the correlation between the energy deposited in the front and back depth segments of the calorimeter for 60 GeV electrons and pions, respectively. The cut labeled **B** corresponding to  $E_f/E_{em} > 0.65$  requires that an electron shower develop early in the calorimeter. Showers surviving both cuts **A** and **B** are found in the lower right corner of the figures. The pion misidentification probability,  $f_{\pi \rightarrow e}$ , is reduced to approximately 0.5% while only an additional 1% of the electrons are lost by the application of cut **B**.

Further improvements in  $e/\pi$  separation are achieved when cuts are made on the shower transverse size. Defining the width  $W$  of a shower as

$$W^2 = \sum_i^{towers} \frac{r_i^2 E_i}{E} - \left( \sum_i^{towers} \frac{r_i E_i}{E} \right)^2,$$

where  $r_i$  is the radius from the shower centroid to the center of tower  $i$ ,  $E_i$  is the energy deposited in tower  $i$  summed over both depth segments and  $E$  is the total shower energy. Distributions of this variable for electrons and pions are plotted in figure 27. The addition of the criterion **C** corresponding to  $W < 2.8$  cm to the remaining sample of pions yields a final result of  $f_{\pi \rightarrow e} = 0.38 \pm 0.07\%$  with a final electron efficiency  $\epsilon = 90\%$ .

## 8 Summary and Acknowledgments

A large, gas sampling electromagnetic calorimeter for the Collider Detector at Fermilab (CDF) has been designed and tested for use in the small angle region between  $2^\circ$  and  $10^\circ$  in polar angle. The sampling layers are constructed using a novel technique in which the insulating side of the cathode pad readout boards is bonded to the proportional tube walls using resistive epoxy. The measured energy response of the calorimeter energy is linear up to 160 GeV and the measured energy resolution is approximately  $25\%/\sqrt{E} + 0.5\%$ . The position resolution varies between 1 mm and 4 mm depending on location in the calorimeter. The calorimeter offers good  $e/\pi$  discrimination, where typically the pion misidentification probability  $f_{\pi \rightarrow e} < 0.5\%$  with electron identification efficiency  $\epsilon > 90\%$ . We wish to thank Jim McElaney and the entire HEPL machine shop crew for their help in constructing these calorimeters. Special thanks must go to Rick Haggerty and Pat Long for their technical contributions. This work was supported primarily by the U. S. Department of Energy under Contracts Nos. DE-AC02-76ER03064 and DE-AC02-76ER03230.

## References

- [1] F. Abe et al., "The Collider Detector at Fermilab", subm. to NIM.
- [2] Phillips Elmet Corporation, Lewiston, Maine.
- [3] Abatron Incorporated, Gilberts, Illinois.
- [4] S. Cihanger et al., "The CDF Forward/Backward Hadron Calorimeter", subm. to NIM.
- [5] Y. Hayshide et al., NIM 216, 127 (1983); NIM 216, 135 (1983);  
Y. Fukui et al., "The CDF End Plug EM Calorimeter", subm. to NIM.
- [6] W.C. Carithers et al., "The CDF End Plug Hadron Calorimeter", subm. to NIM.
- [7] G. Drake et al., "CDF Front End Electronics: The RABBIT System", subm to NIM.
- [8] E. Barsotti et al., "FASTBUS Data Acquisition System for CDF", subm. to NIM.
- [9] J. Saarloos et al., "High Voltage Control and Monitoring System for Proportional Chambers", subm. to IEEE Nucl. Sci. Symp., Oct. 1987.
- [10] M. Atac, "Wire Chamber Aging and Wire Material", IEEE Trans. on Nucl. Sci. NS34, 476 (1987).
- [11] Y. Fukui et al., Gas Sampling Calorimeter Workshop II, Fermilab (1985), p. 1.

# Table

Cut	$e$ efficiency	$\pi$ misidentification probability $f_{\pi \rightarrow e}$ (%)	
	$\epsilon$ (%)	30 GeV	60 GeV
A	95.	$2.9 \pm 0.2$	$1.5 \pm 0.1$
A + B	94.	$0.98 \pm 0.08$	$0.53 \pm 0.05$
A + B + C	90.	$0.43 \pm 0.09$	$0.38 \pm 0.07$

Table 1: Results on  $e/\pi$  discrimination at 30 and 60 GeV. The cuts are described in the text.

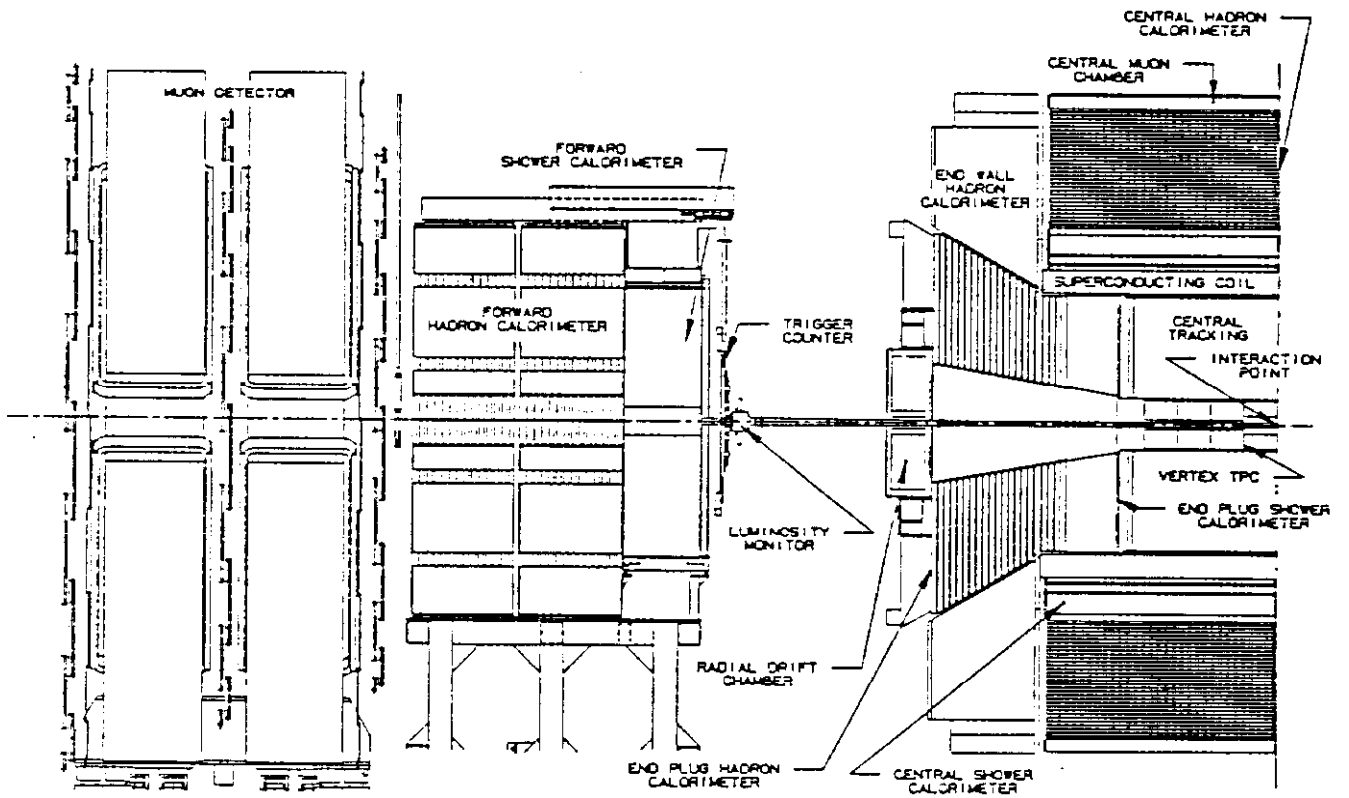


Figure 1: Side view of the forward half of the CDF detector. The forward electromagnetic calorimeter is approximately 6.5 m from the nominal beam-beam interaction point.

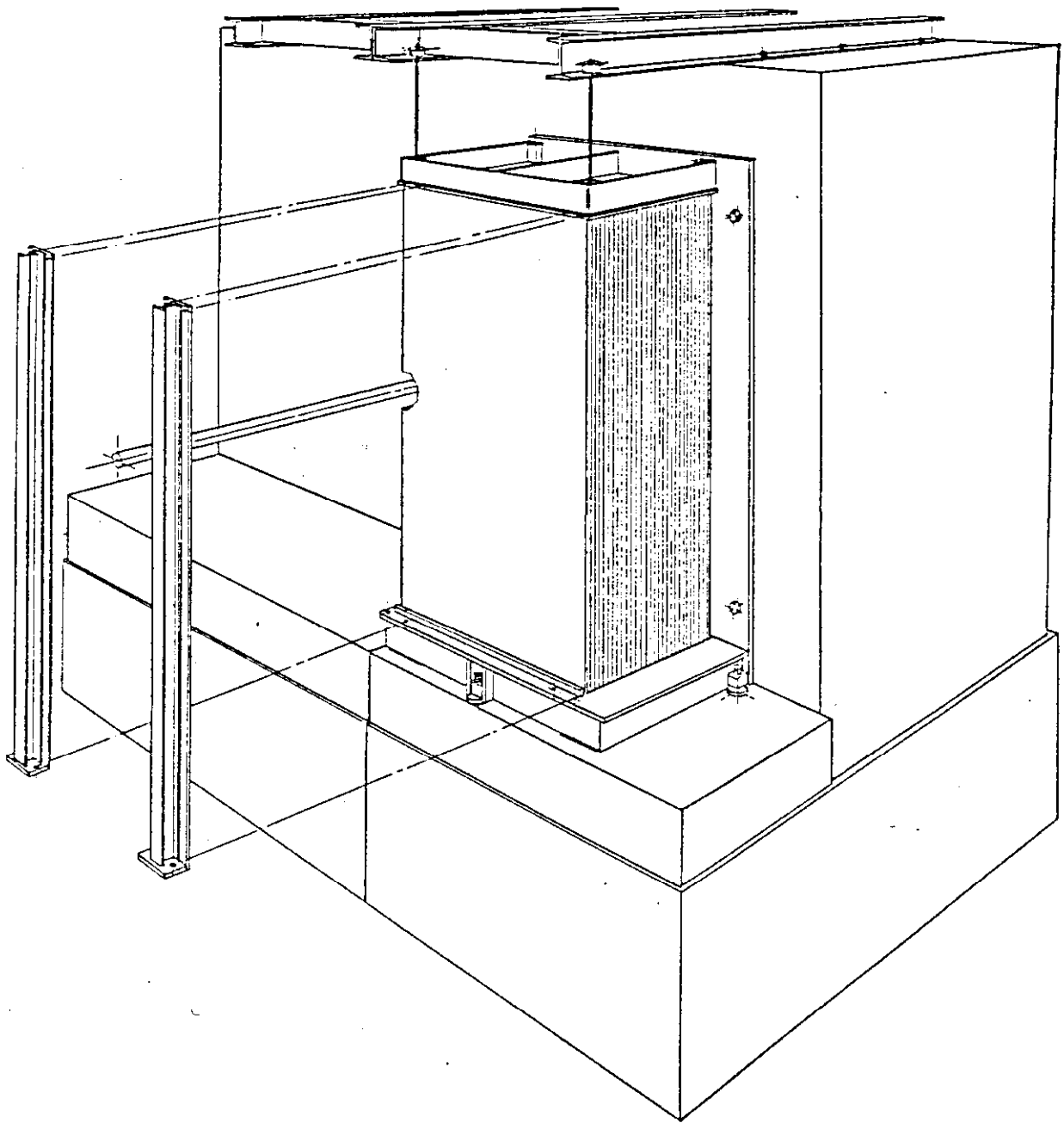


Figure 2: One half of one end of the forward electromagnetic calorimeter shown mounted on the front face of the forward hadron calorimeter steel.

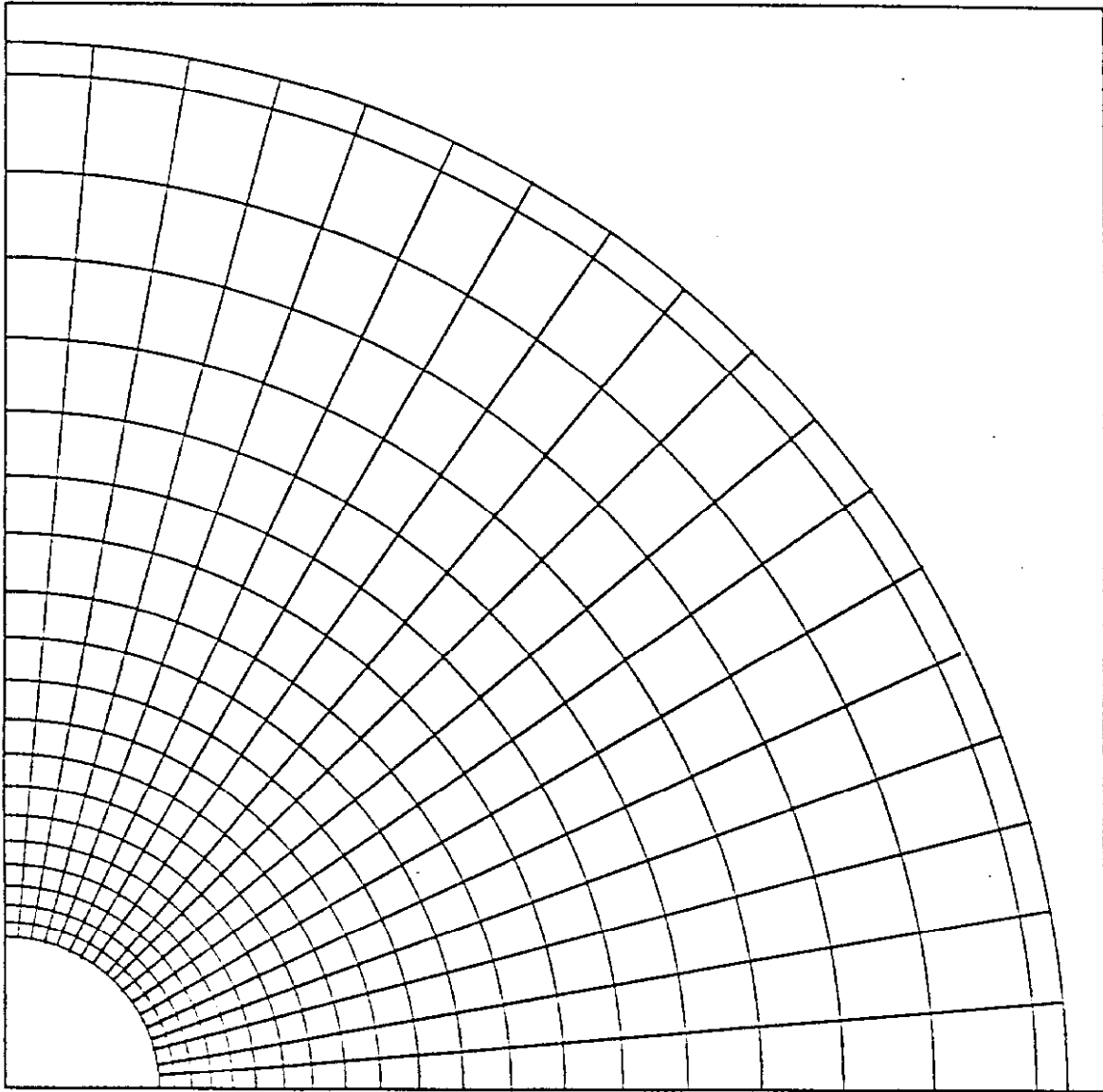


Figure 3: The pad geometry of a chamber at layer 10 within the calorimeter

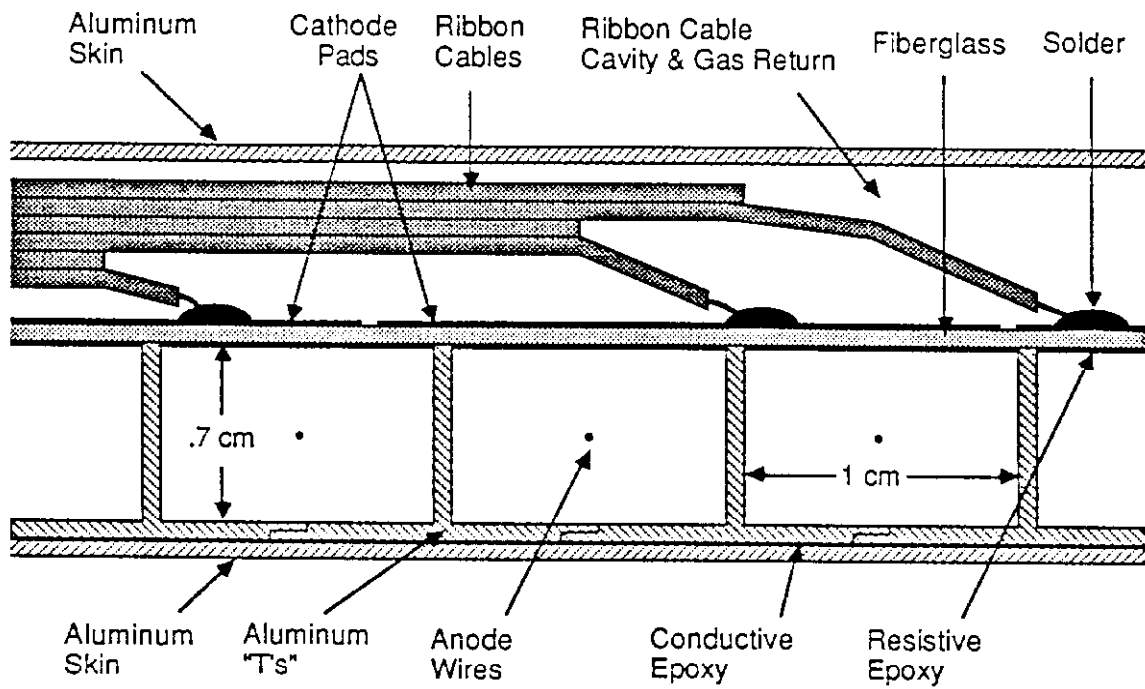


Figure 4: Cross section of a typical chamber with appropriate dimensions indicated.

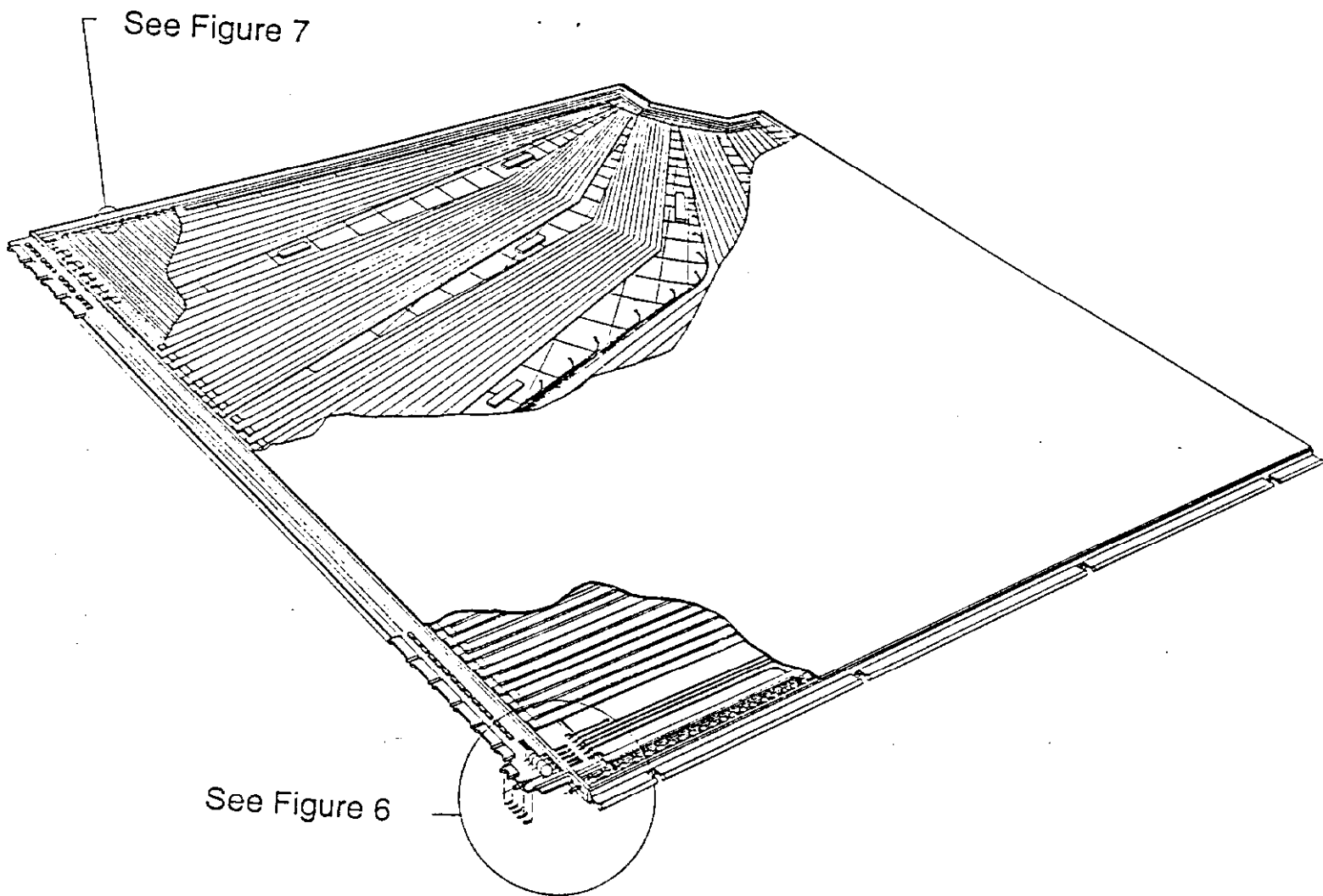
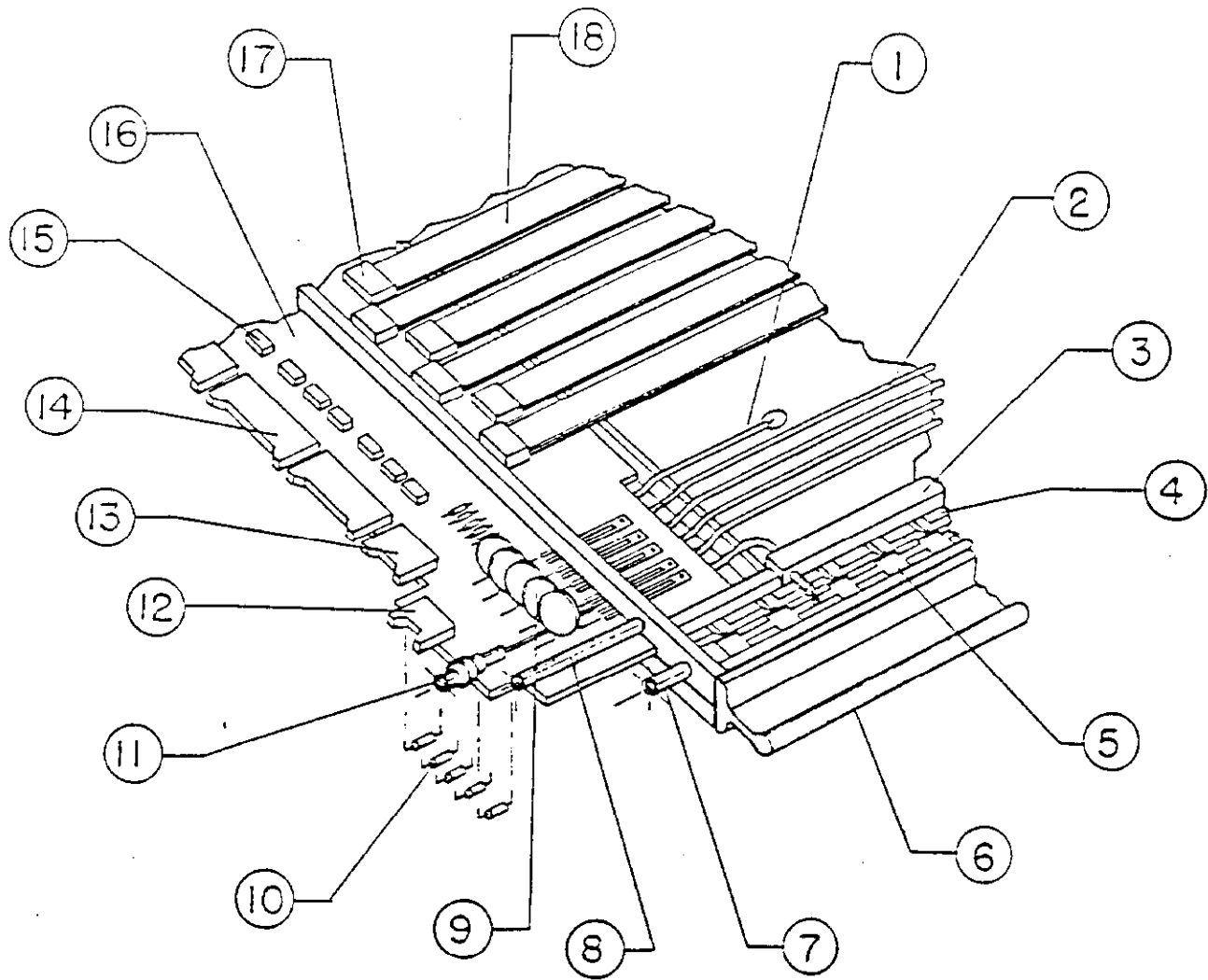
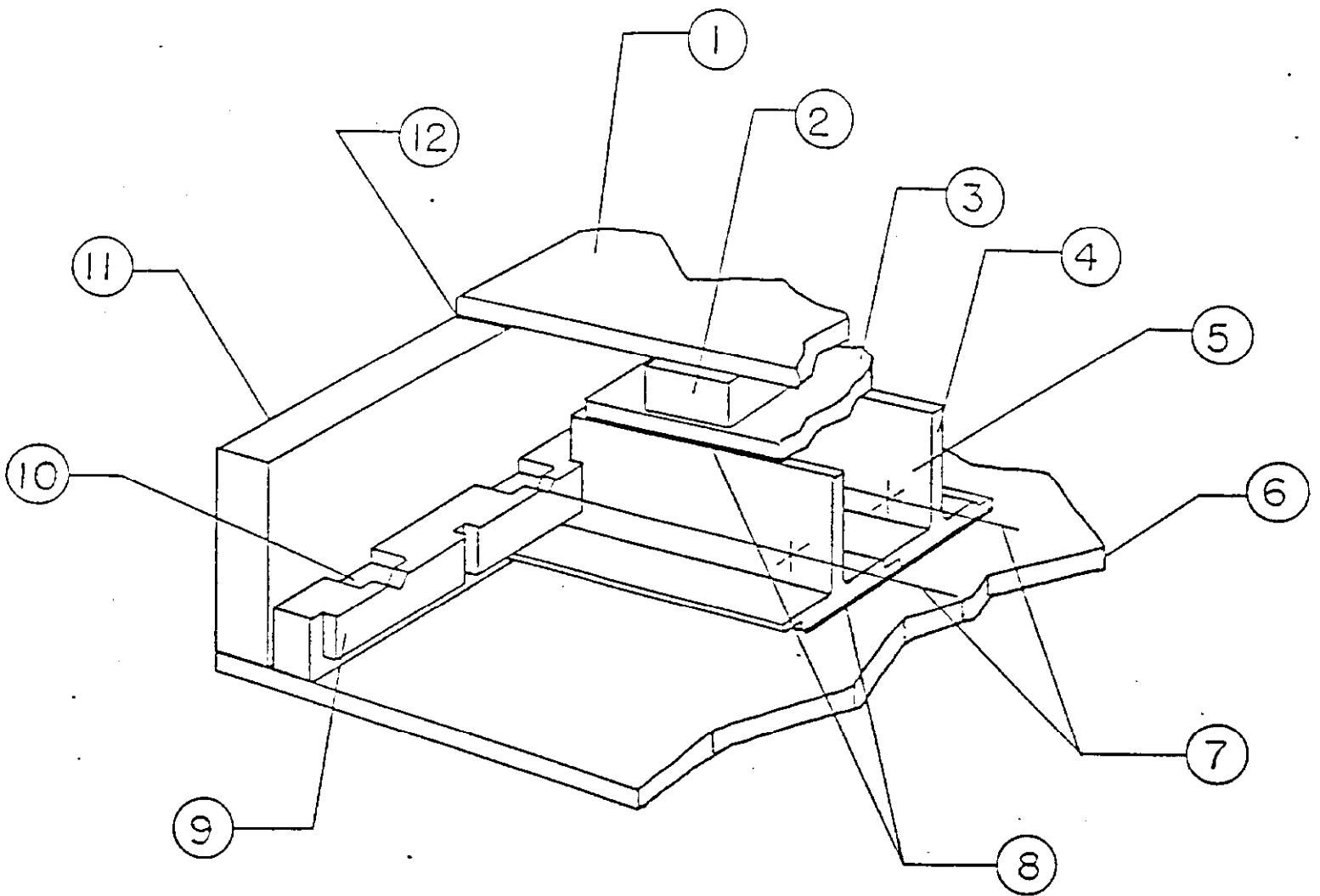


Figure 5: Cutaway view of a chamber. Details of the chamber construction are illustrated in figures 6 and 7.



1. Ground Strap
2. Internal High Voltage Leads
3. Fiberglass Gas Baffle
4. Molded Plastic Wire Guide
5. Anode Wire High Voltage Bus
6. Plastic Hanger/Guide Rail
7. Gas Inlet
8. Gas Outlet
9. Anode Signal Blocking Capacitors
10. High Voltage Protection Resistors
11. High Voltage Connector
12. Anode Signal Readout Connector
13. Guard Ring Readout Connector
14. Cathode Pad Readout Connector
15. Series Resistor Packs
16. Fiberglass Cable Connector Strip
17. Ribbon Cable Connectors
18. Ribbon Cable Harness

Figure 6: Transition strip detail of a chamber. The various components are illustrated in the figure.



1. Aluminum Lid
2. Fiberglass Gas Baffle
3. Cathode Pad Panel
4. Extruded Aluminum "T"
5. Proportional Tube Cell
6. Aluminum Sheet
7. Gold-Plated Tungsten Wire (50 microns)
8. Resistive Epoxy Coating (50 microns)
9. Molded Plastic Wire Guide
10. Anode Wire Solder Pad
11. Fiberglass Chamber Edge Frame
12. Urethane Epoxy Gas Seal

Figure 7: Proportional tube detail of a chamber. The various components are illustrated in the figure.

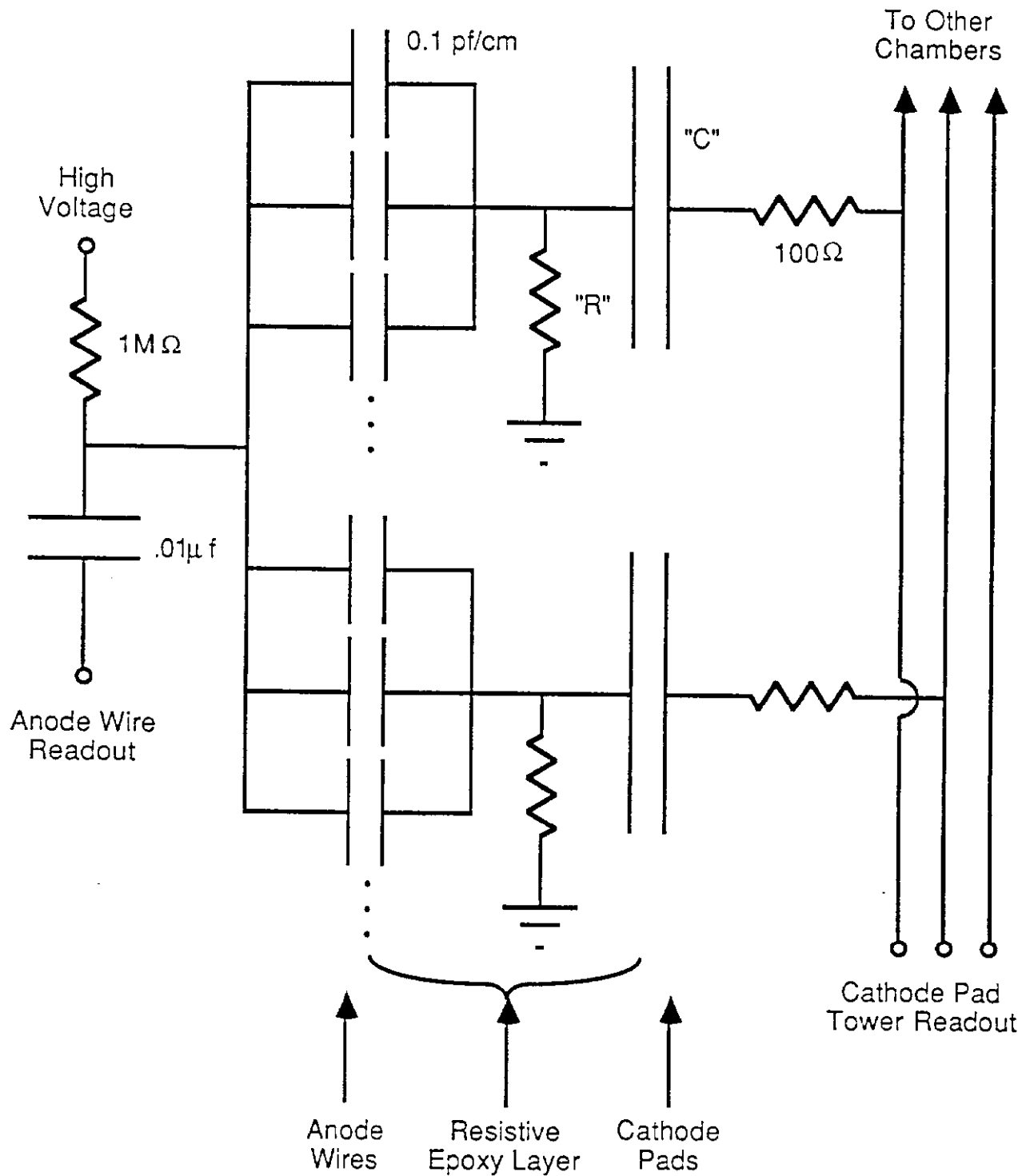


Figure 8: Effective circuit diagram for a calorimeter chamber illustrating the lumped "RC" effect of the resistive epoxy layer.

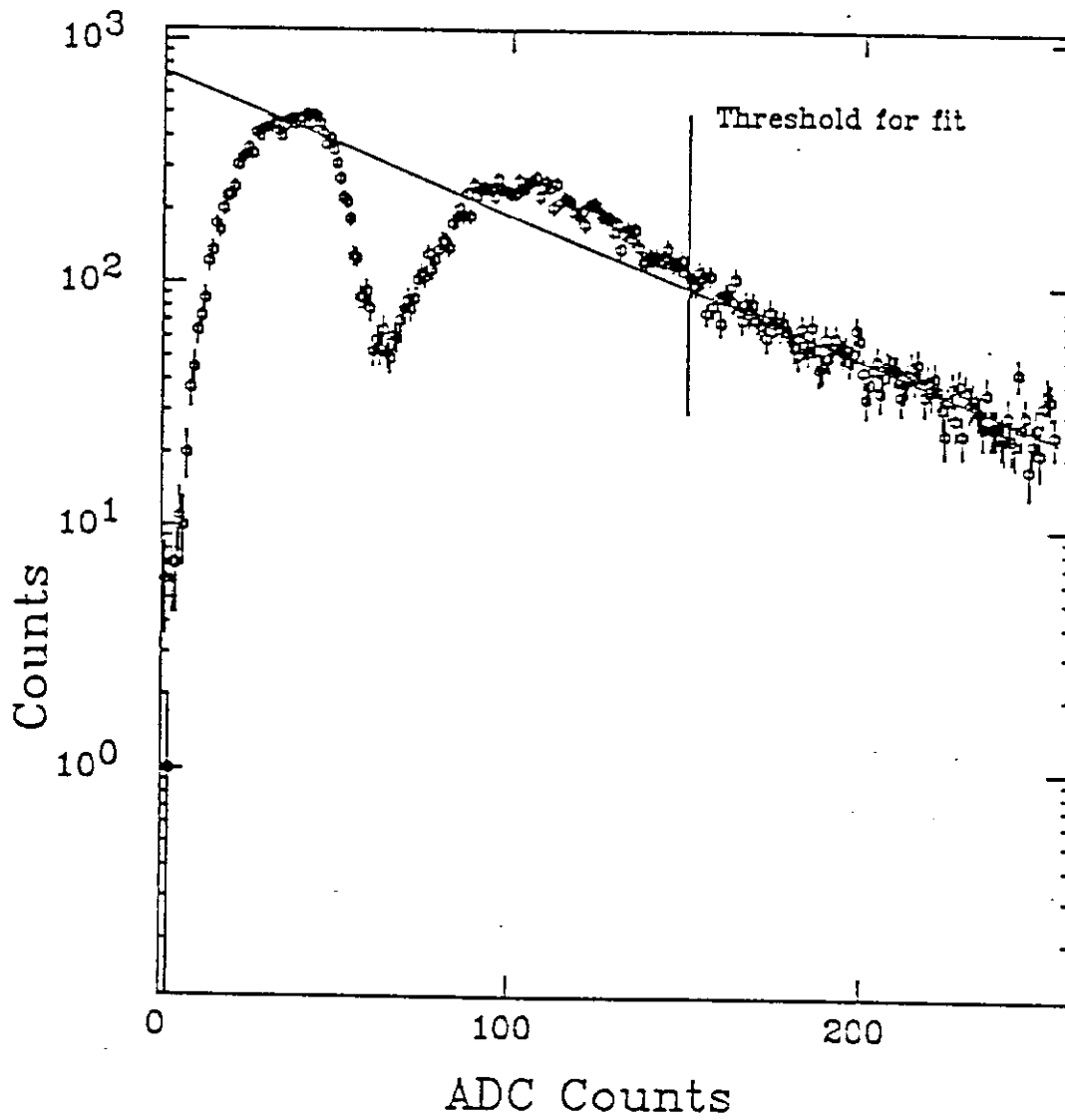


Figure 9:  $^{106}\text{Ru}$  charge distribution. The spectrum is fit above the cut to an exponential and the coefficient is used as a measure of gain.

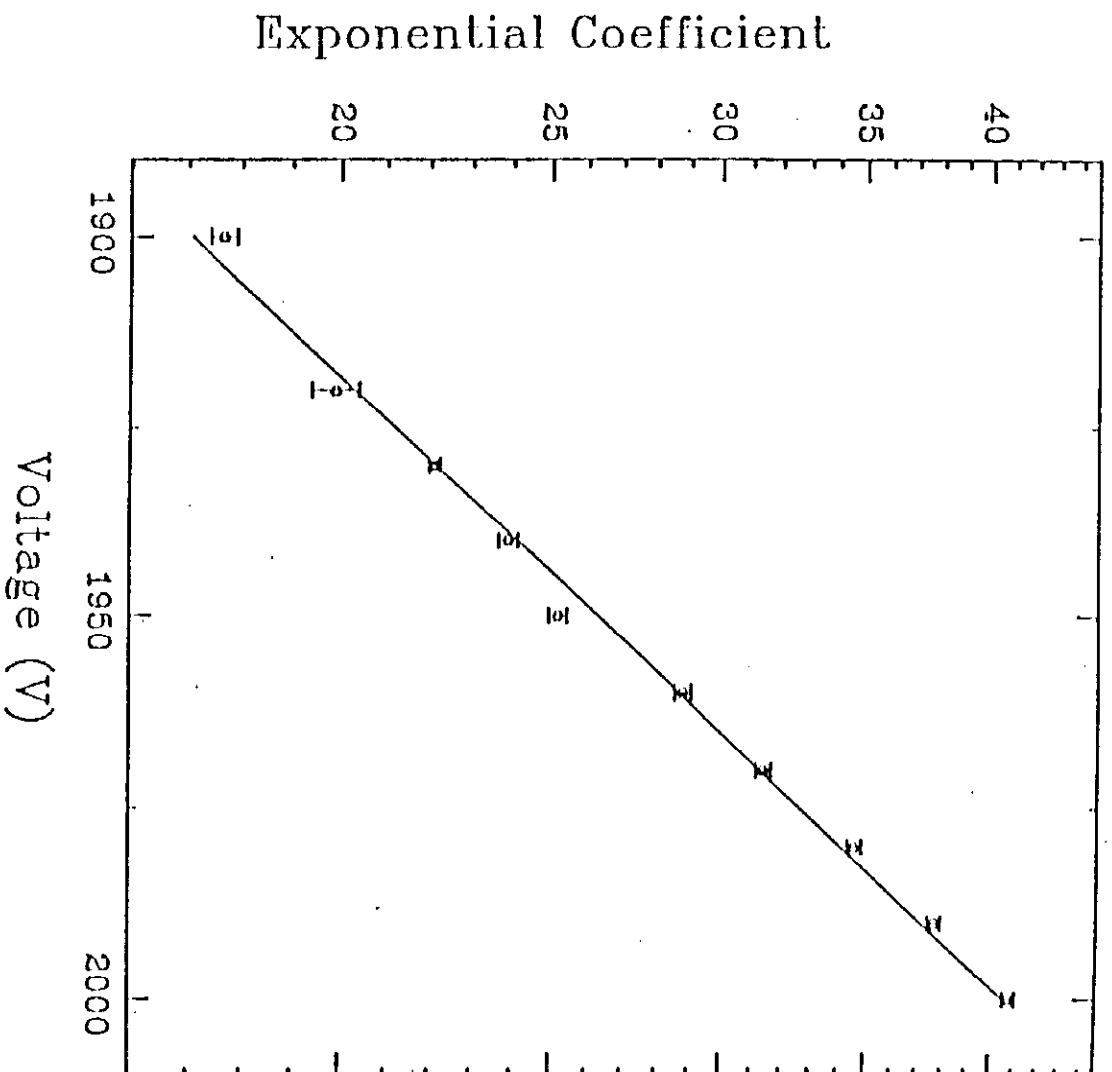


Figure 10: High Voltage response of  $^{106}\text{Ru}$  spectrum illustrating gain dependence of the exponential slope.

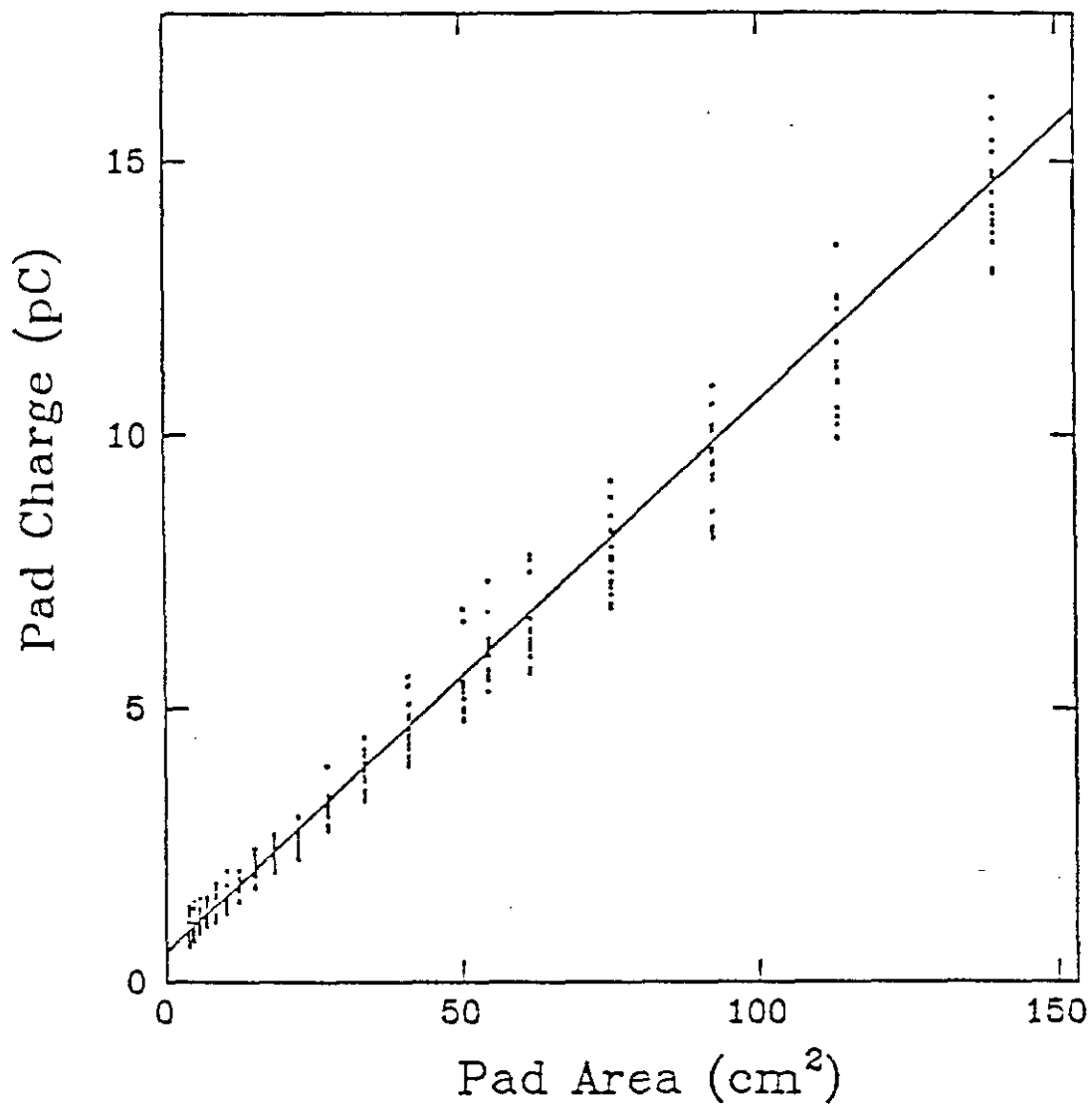


Figure 11: Pulse test of a chamber, showing the ratio of the induced charge to the applied voltage step. The line is calculated from an electrostatics model using the known chamber geometry.

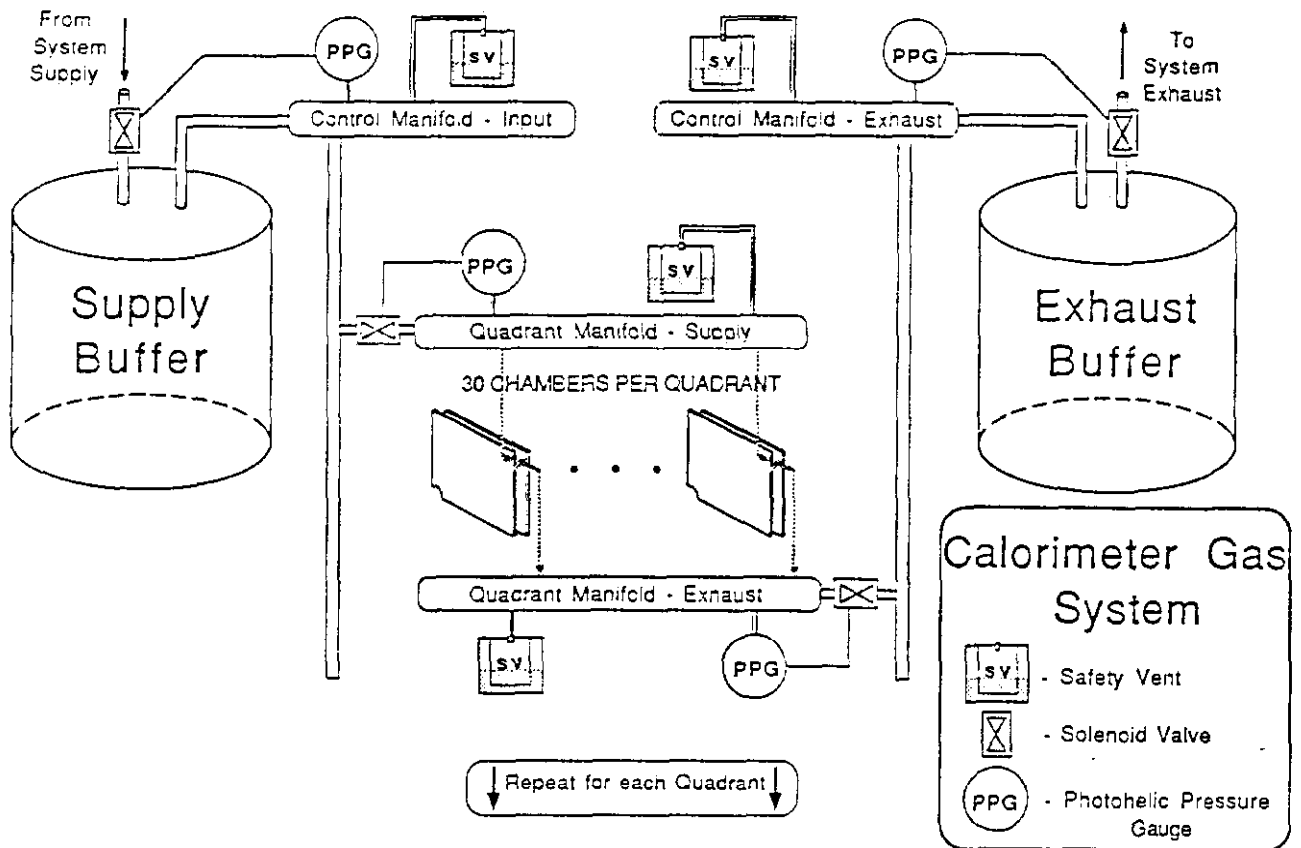


Figure 12: Block diagram illustrating gas system flow. The diagram illustrates the gas system for one end of the forward electromagnetic calorimeter.

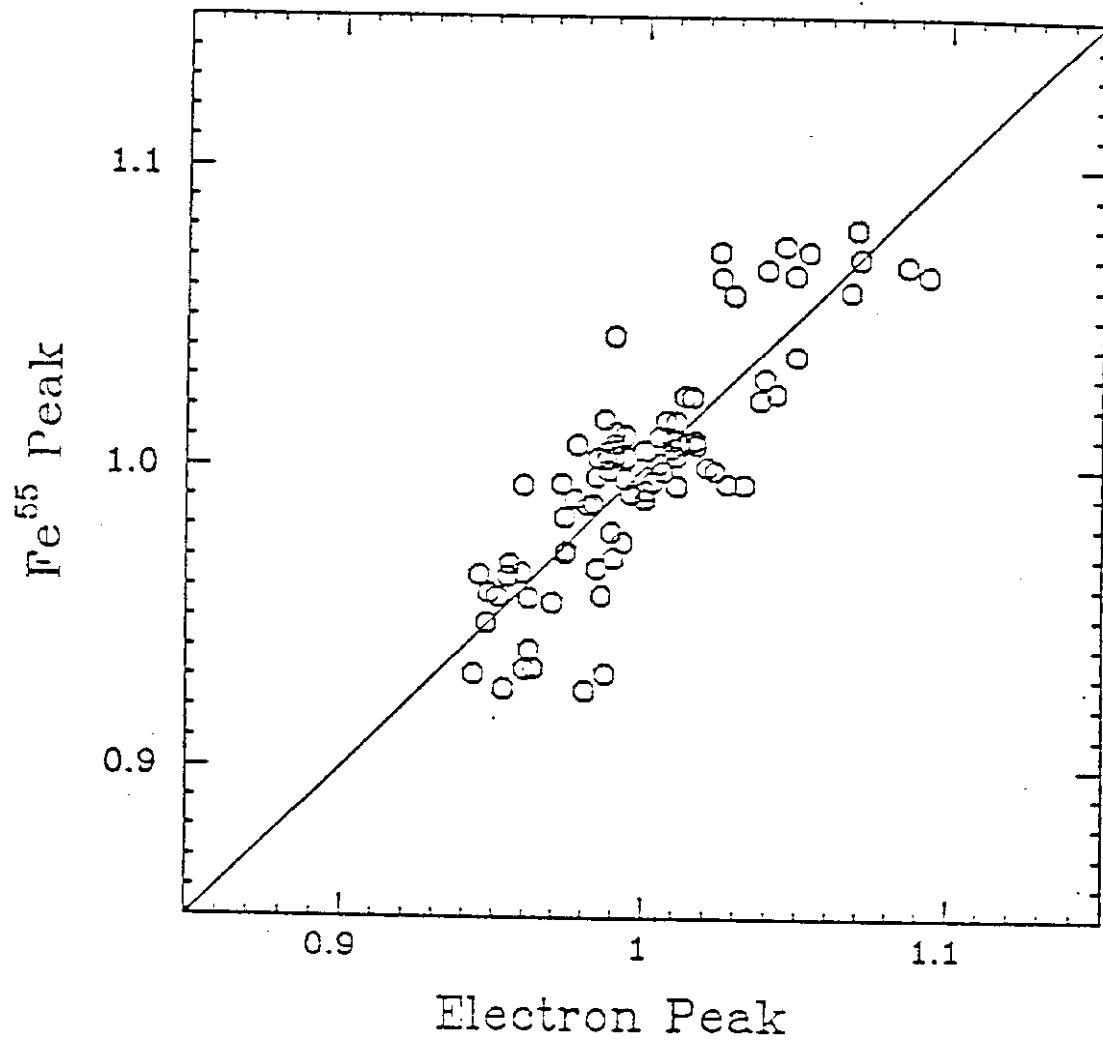


Figure 13: Correlation between fluctuations in calorimeter gain with monitor tube gain.

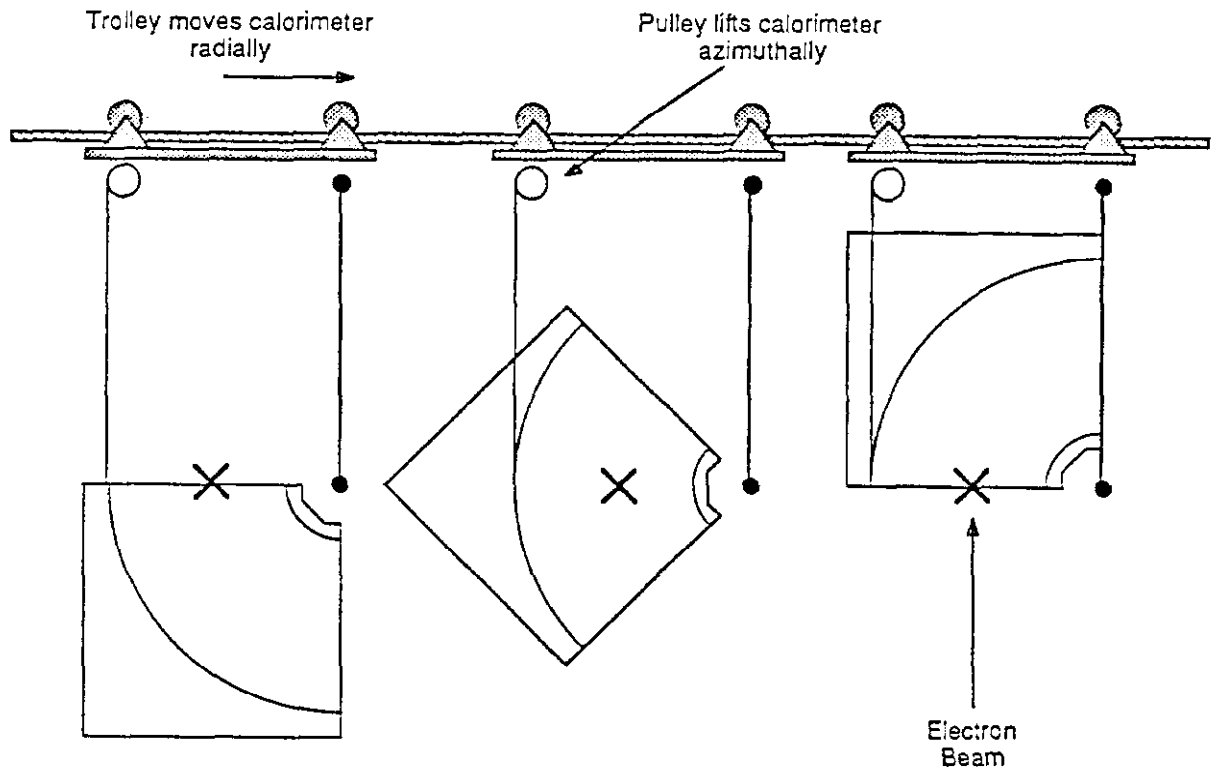


Figure 14: Calorimeter as mounted in the test beam to allow alignment of the tower geometry with beam.

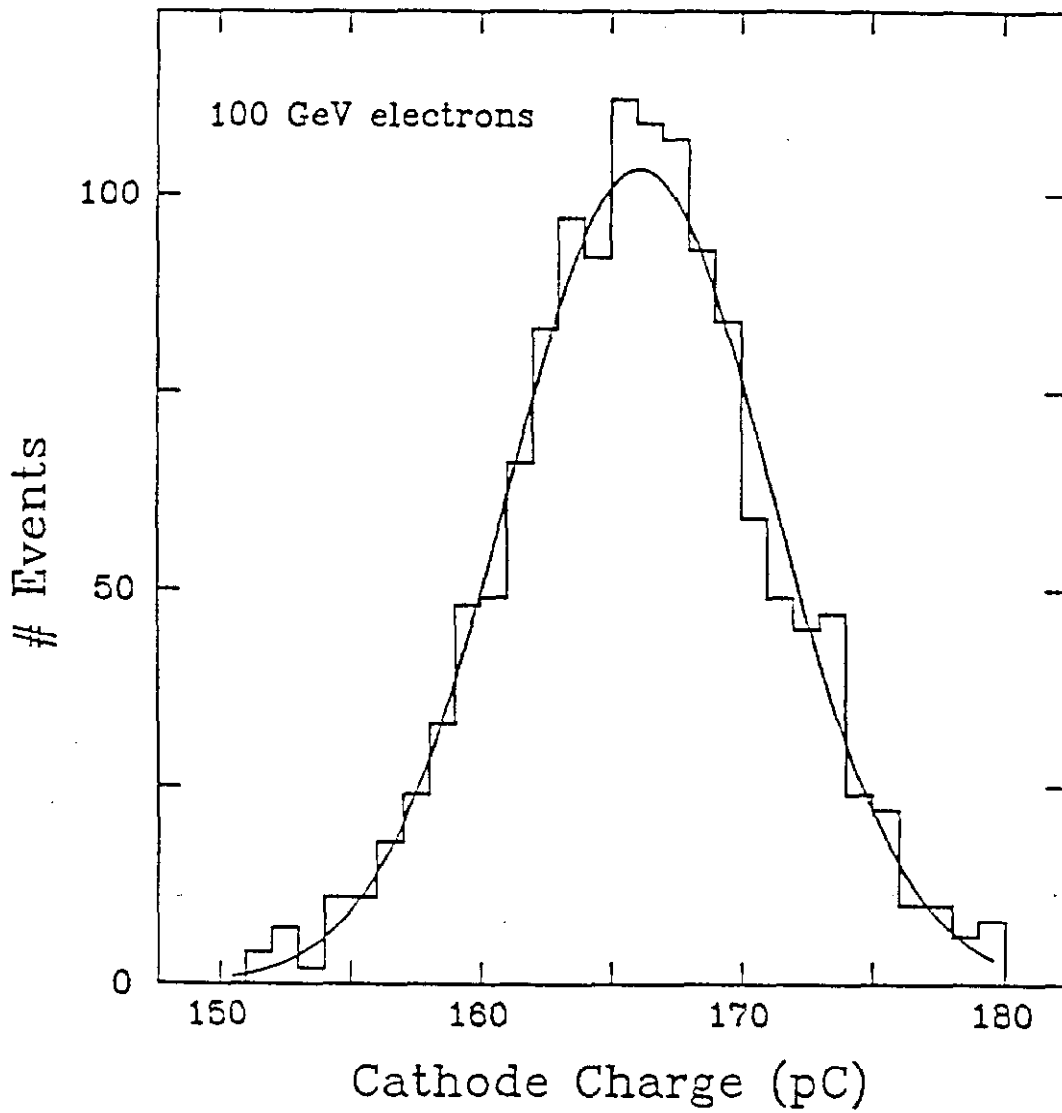


Figure 15: Cathode charge measured from sample of 100 GeV electrons. Gaussian fit is overlaid.

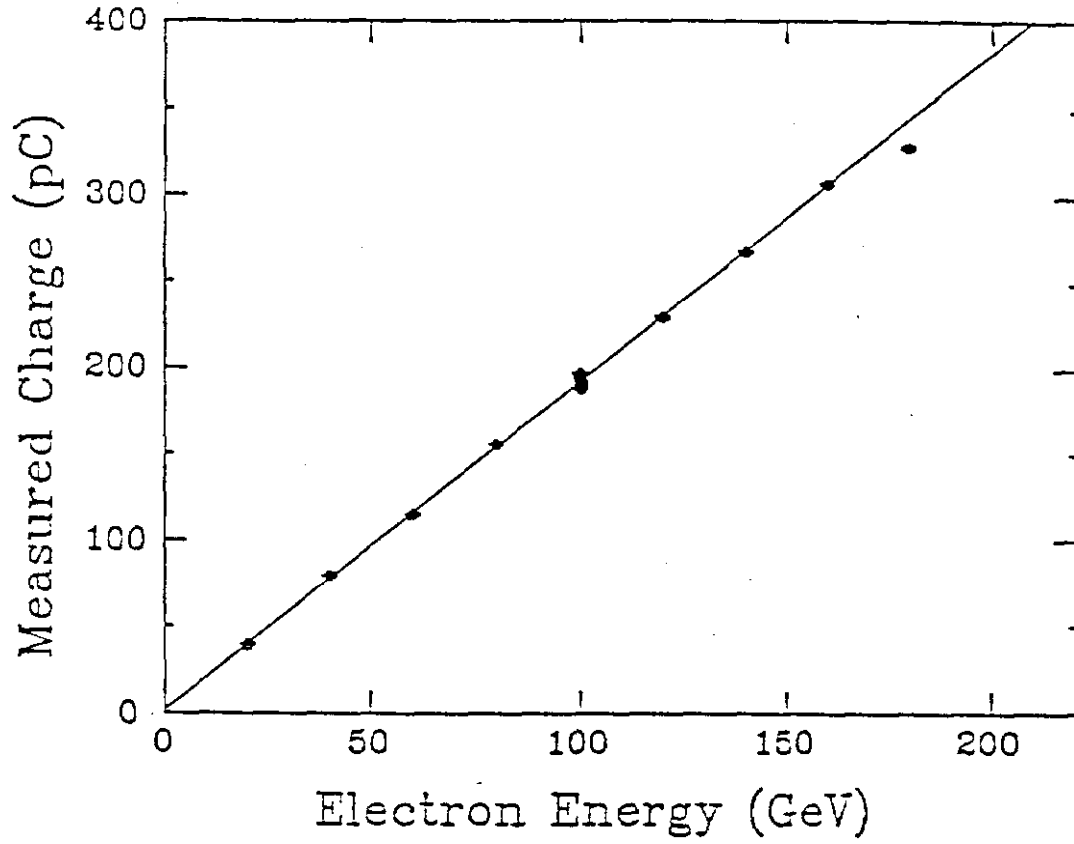


Figure 16: Calorimeter response as a function of incident electron energy. The data from the cathode pads are plotted.

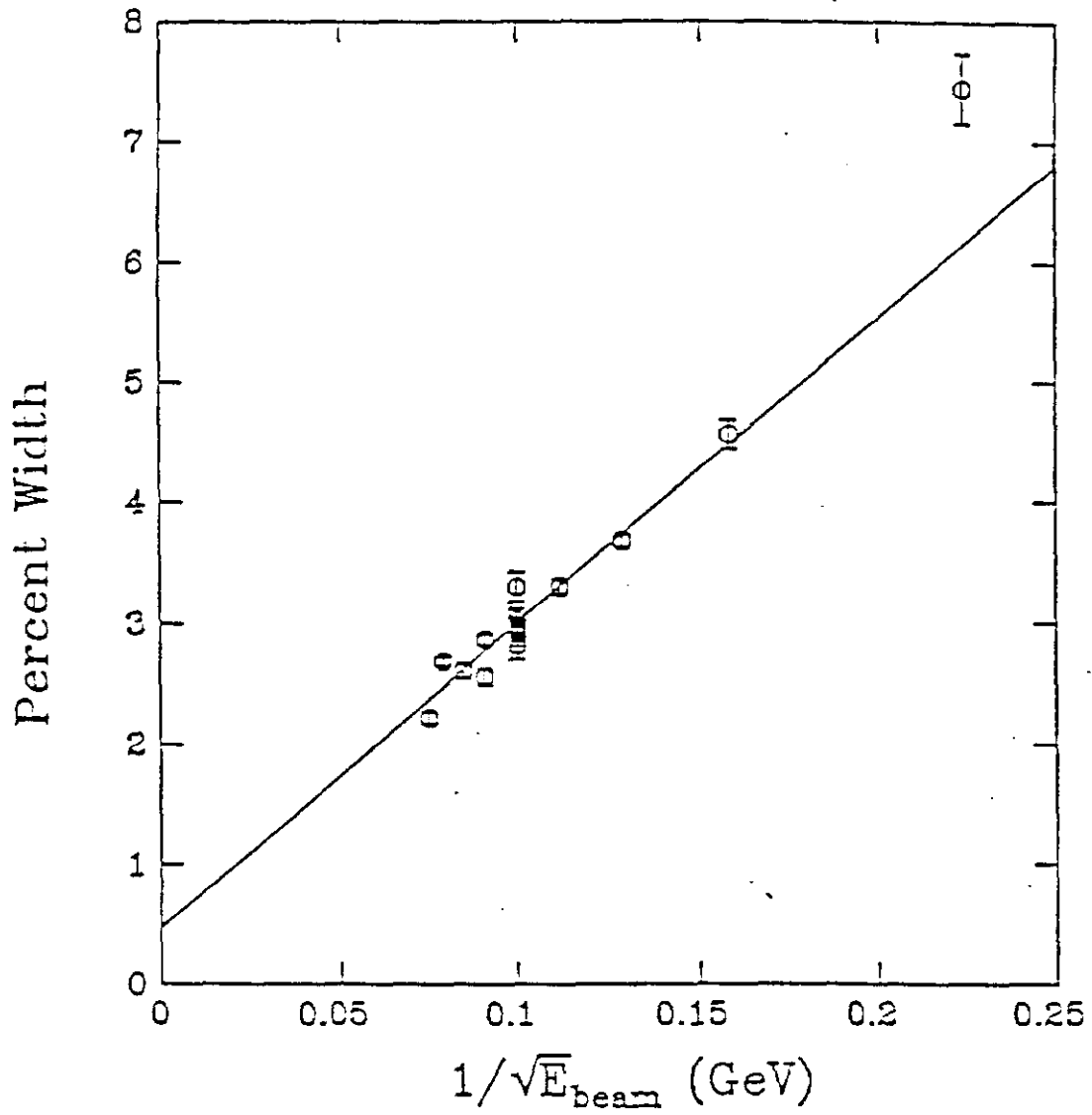


Figure 17: Measured energy response as a function of  $1/\sqrt{E}$ . The line is described in the text.

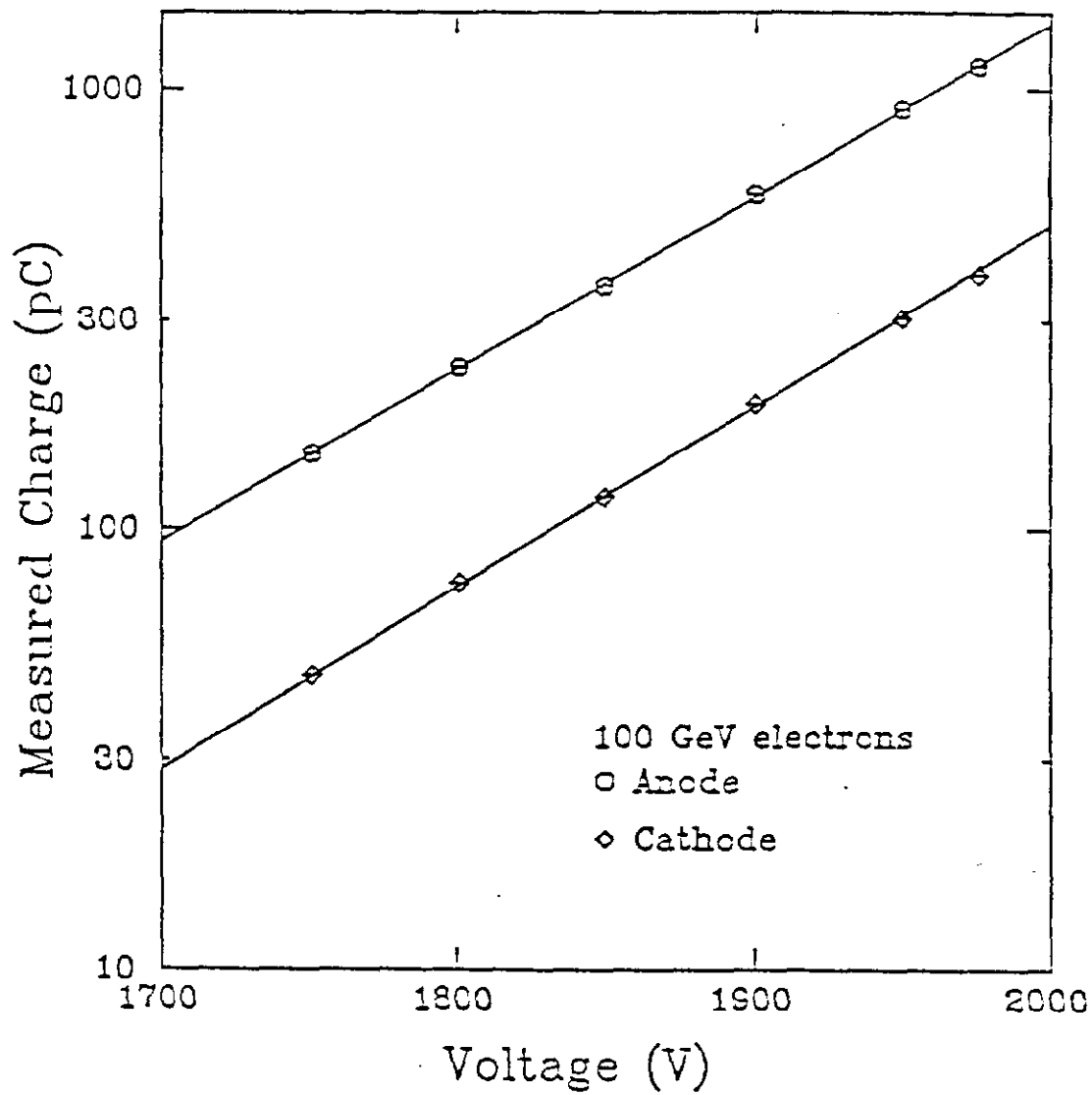


Figure 18: Calorimeter response as a function of voltage. The data are plotted separately for the pad sum and the wire sum.

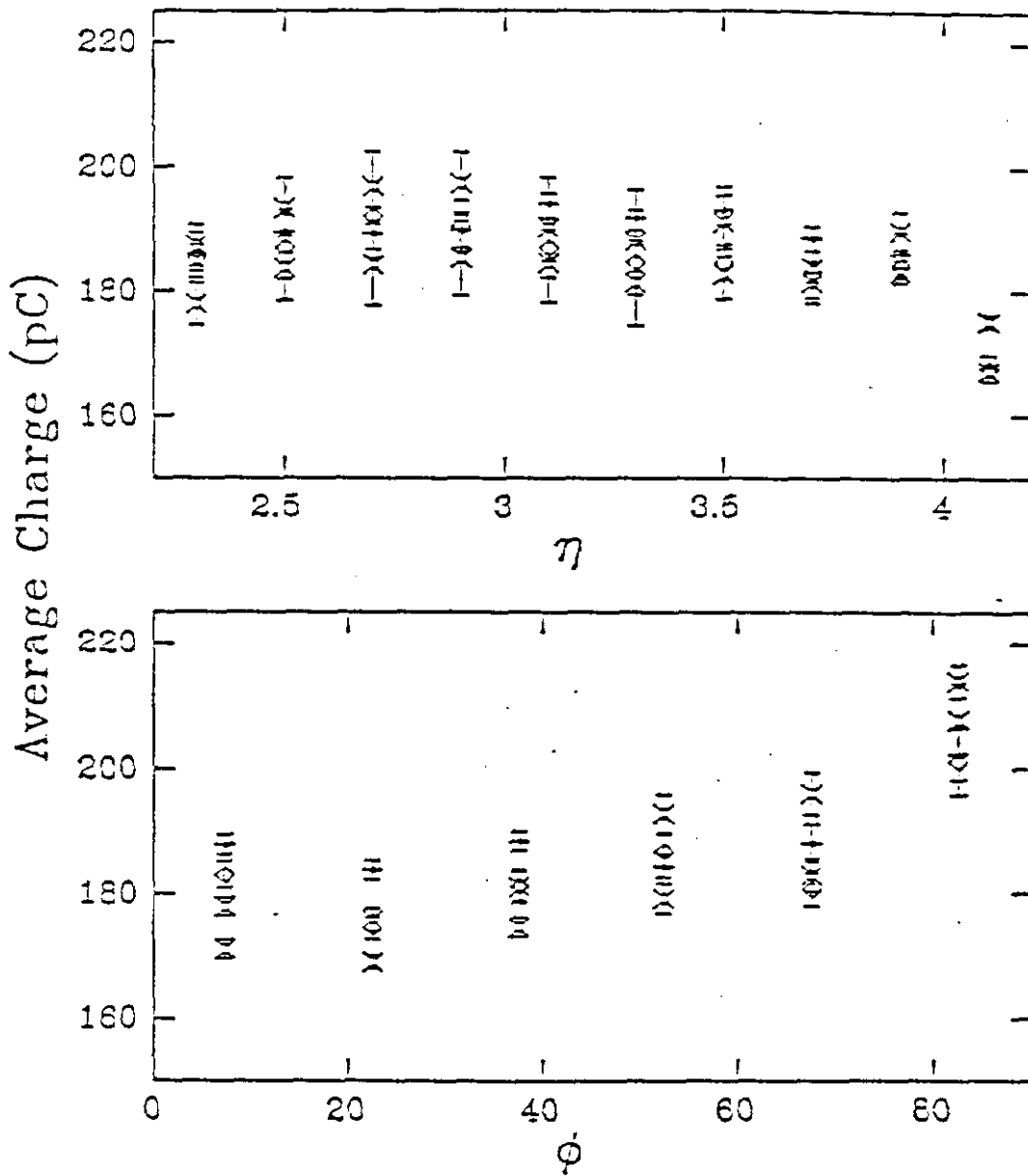


Figure 19: Calorimeter response as a function of  $\eta$  and  $\phi$ . Four sets of data from three different quadrants are overlaid.

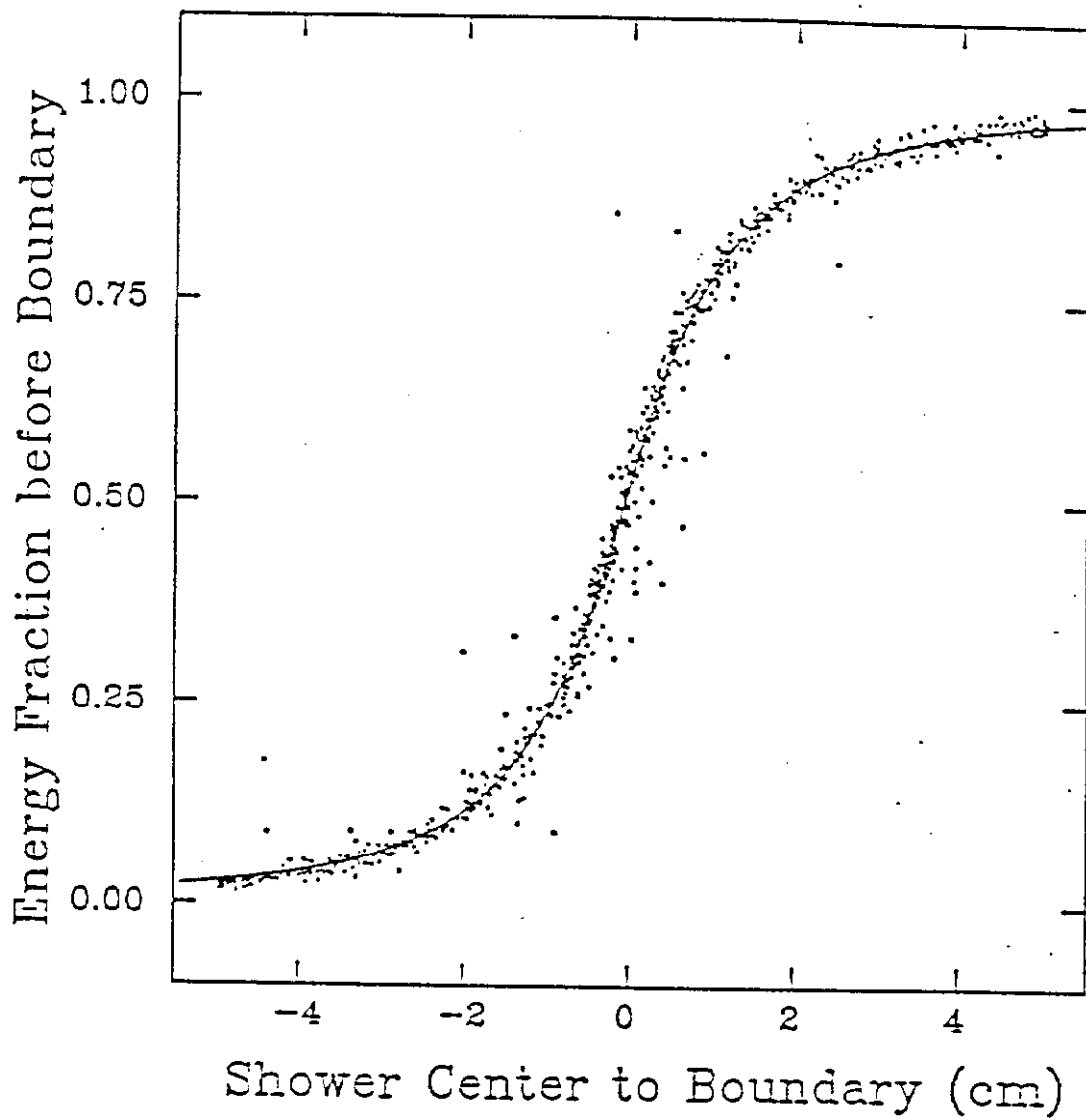


Figure 20: Fraction of charge on one side of tower boundary as a function of distance of the electron from that boundary. The curve is the integral of the transverse shower profile.

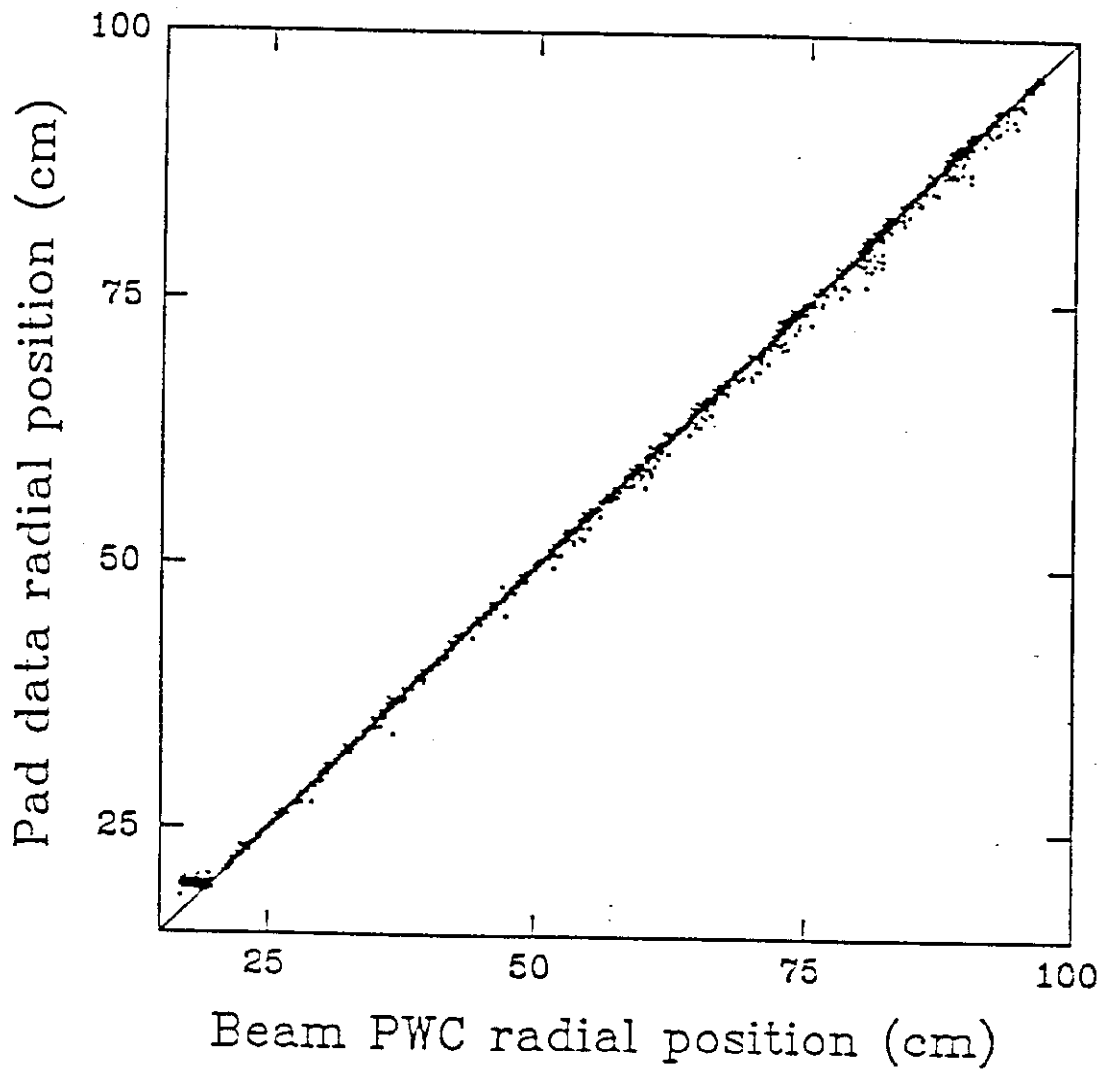


Figure 21: Reconstructed electron shower position as a function of beam PWC position.

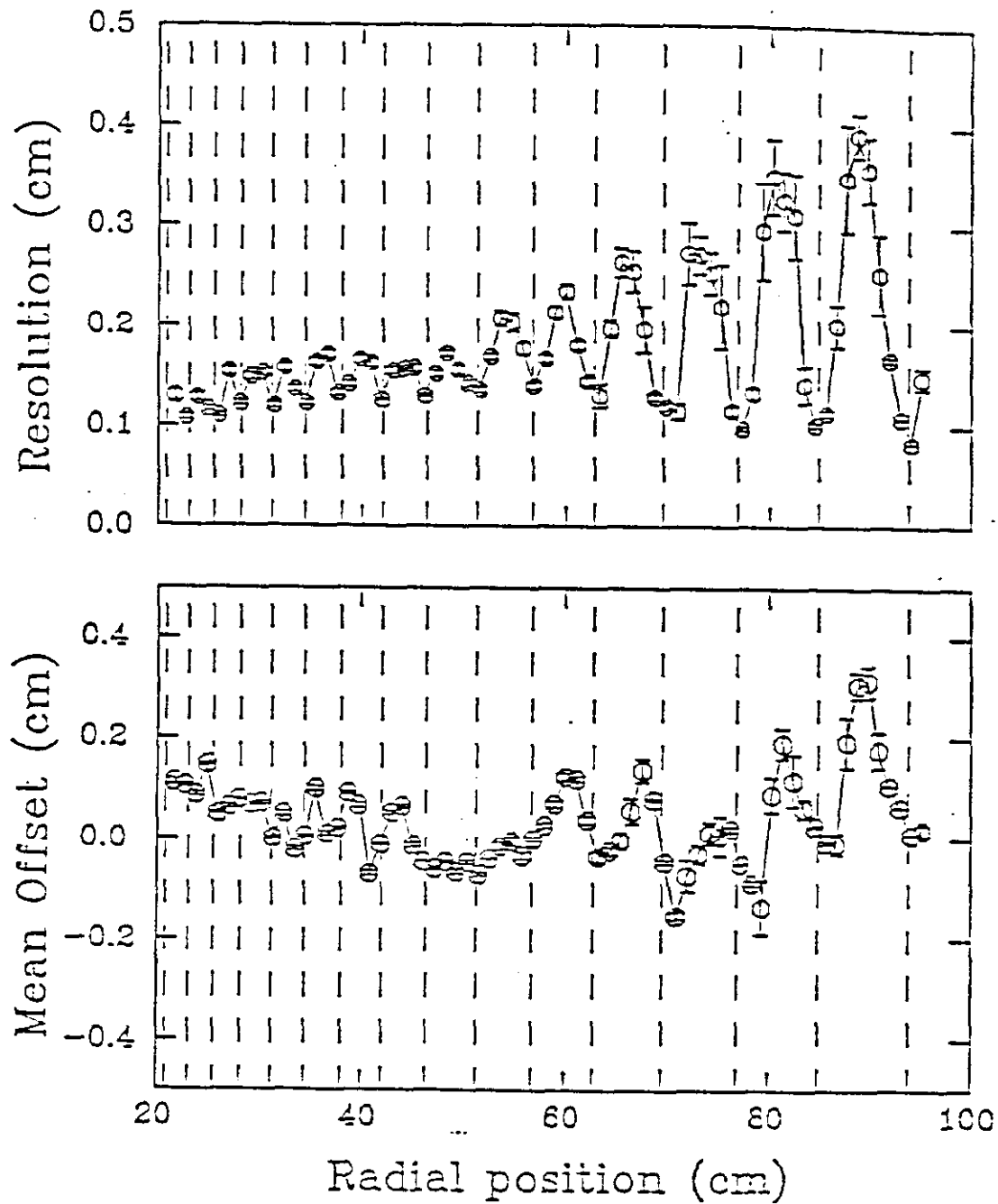


Figure 22: Position resolution and offset across the face of the calorimeter. The dashed lines indicate pad boundaries.

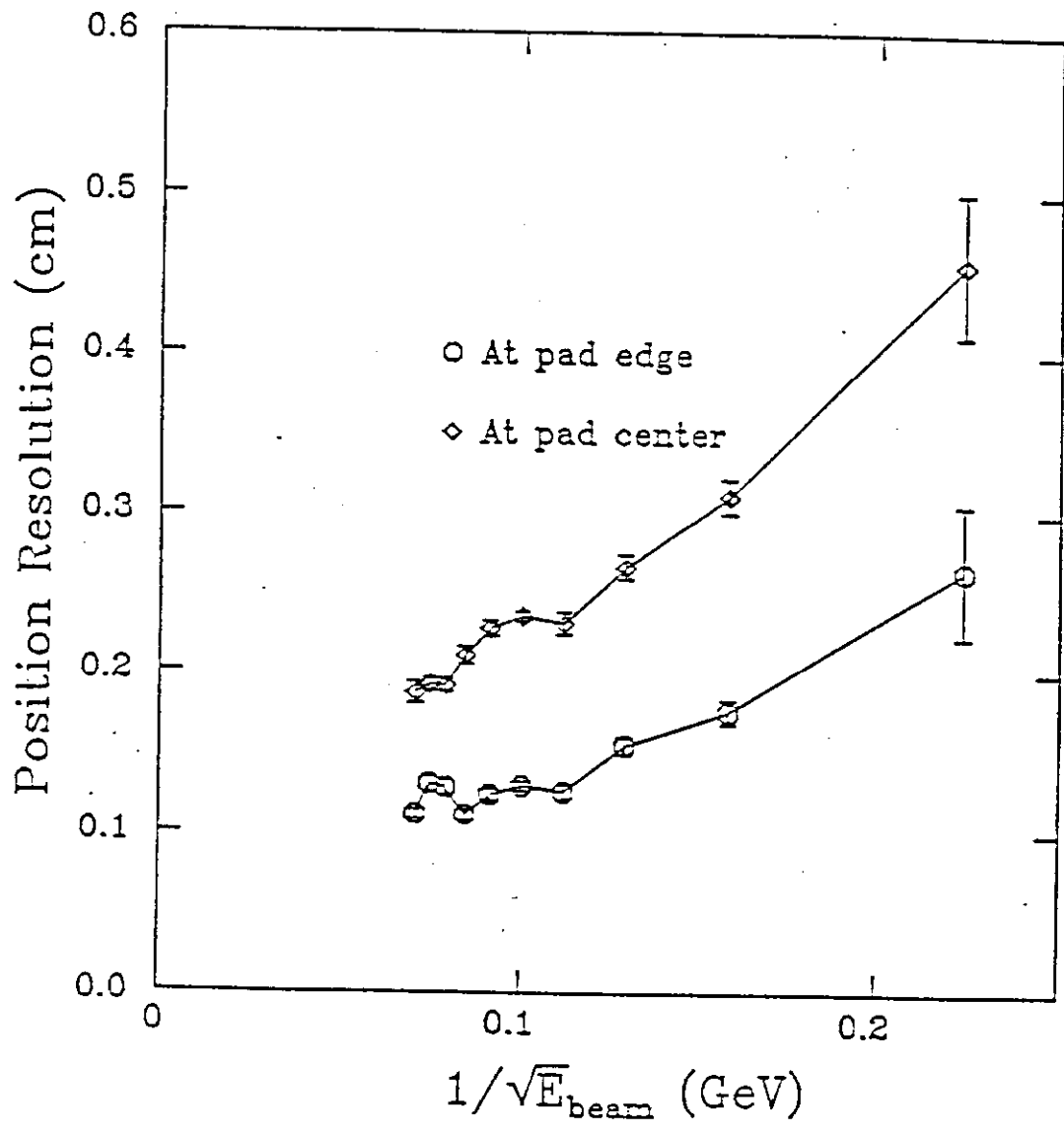


Figure 23: Energy dependence of position resolution. The position resolution is markedly worse for low energy showers.

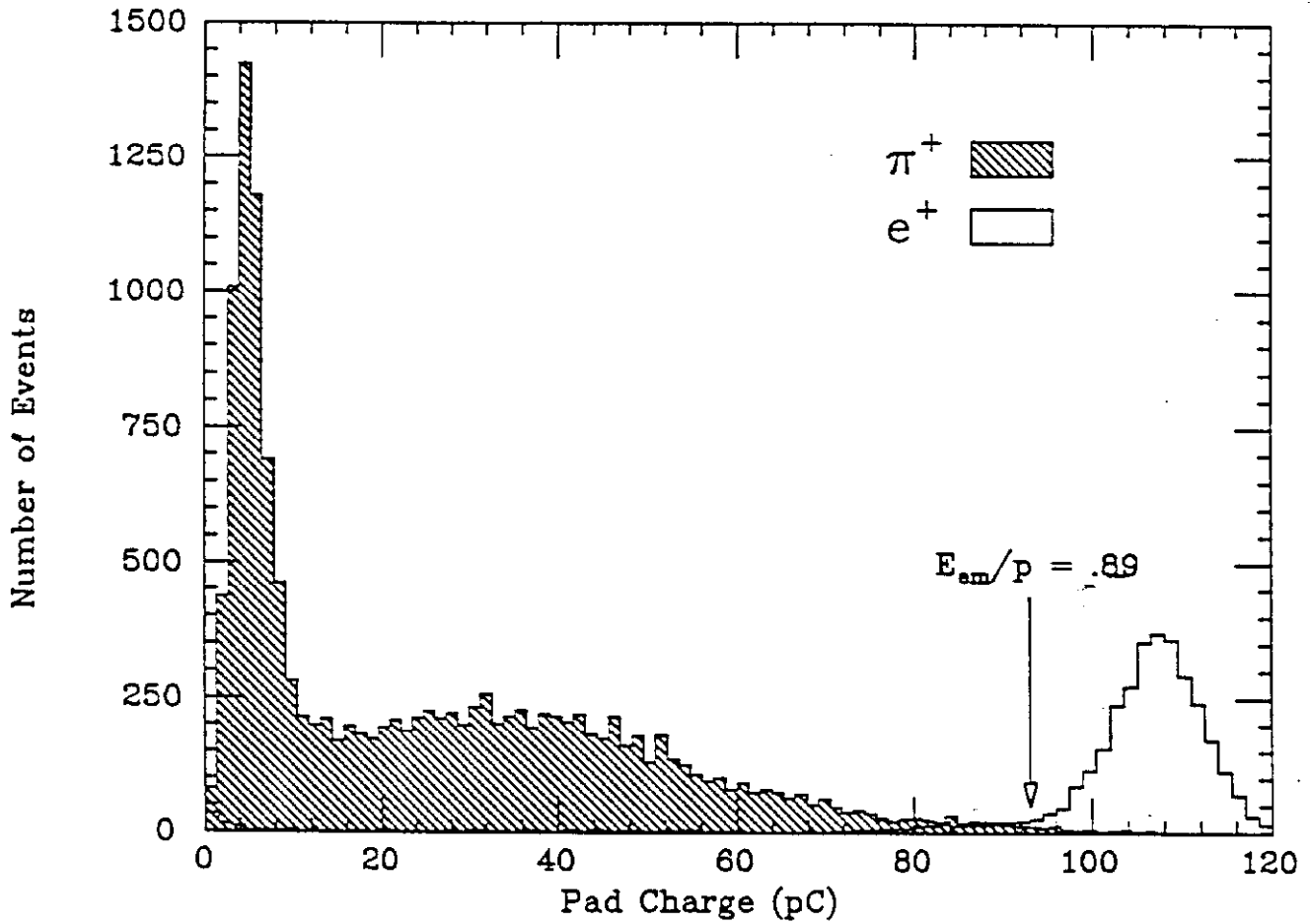


Figure 24: Distribution of energy in electromagnetic calorimeter divided by measured momentum for electrons and pions. This is equivalent to  $E_{em}/E$ . The cut A is displayed.

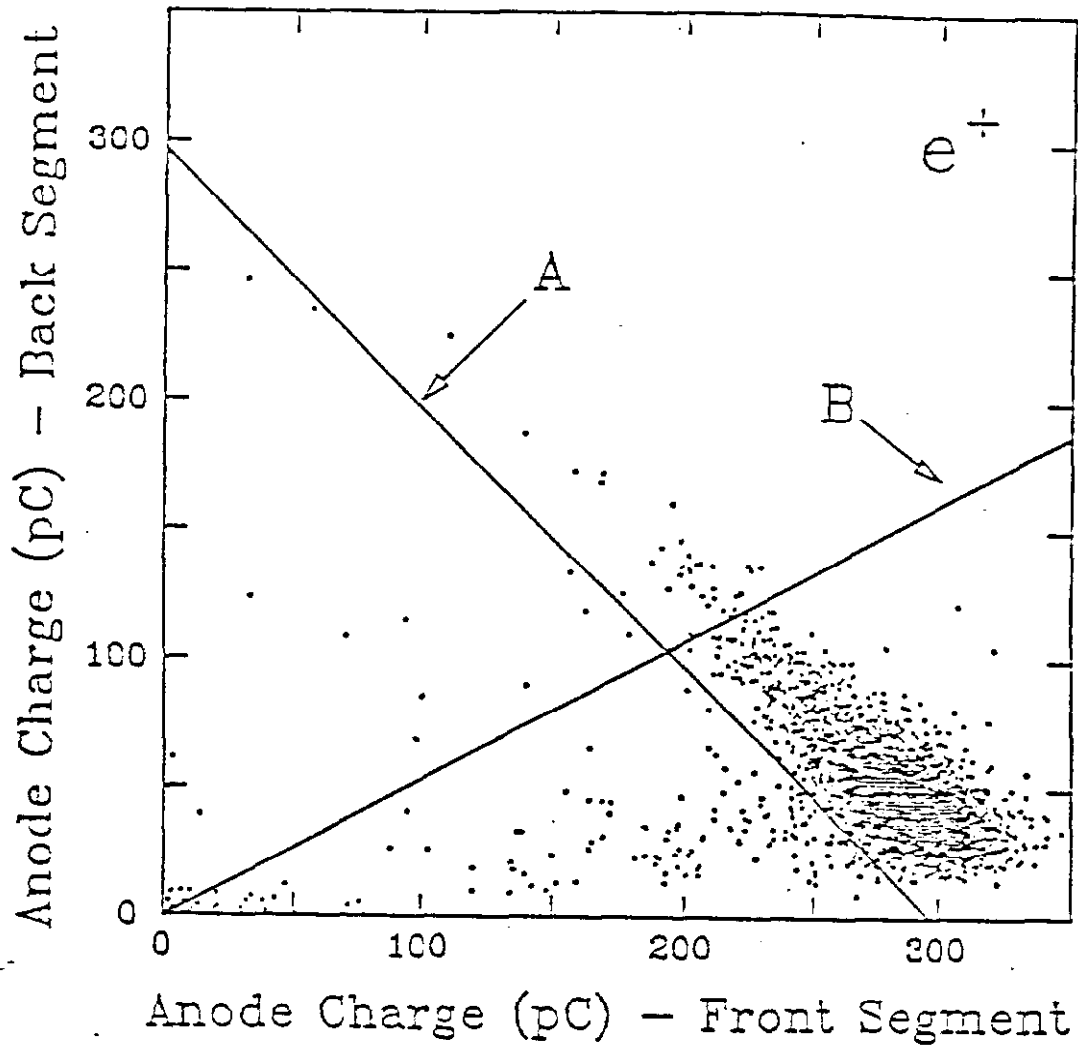


Figure 25: Energy in front half of electromagnetic calorimeter versus energy in back half for 60 GeV electrons. Solid lines correspond to cuts A and B as discussed in the text. Events surviving both cuts are to the right of line A and below line B respectively.

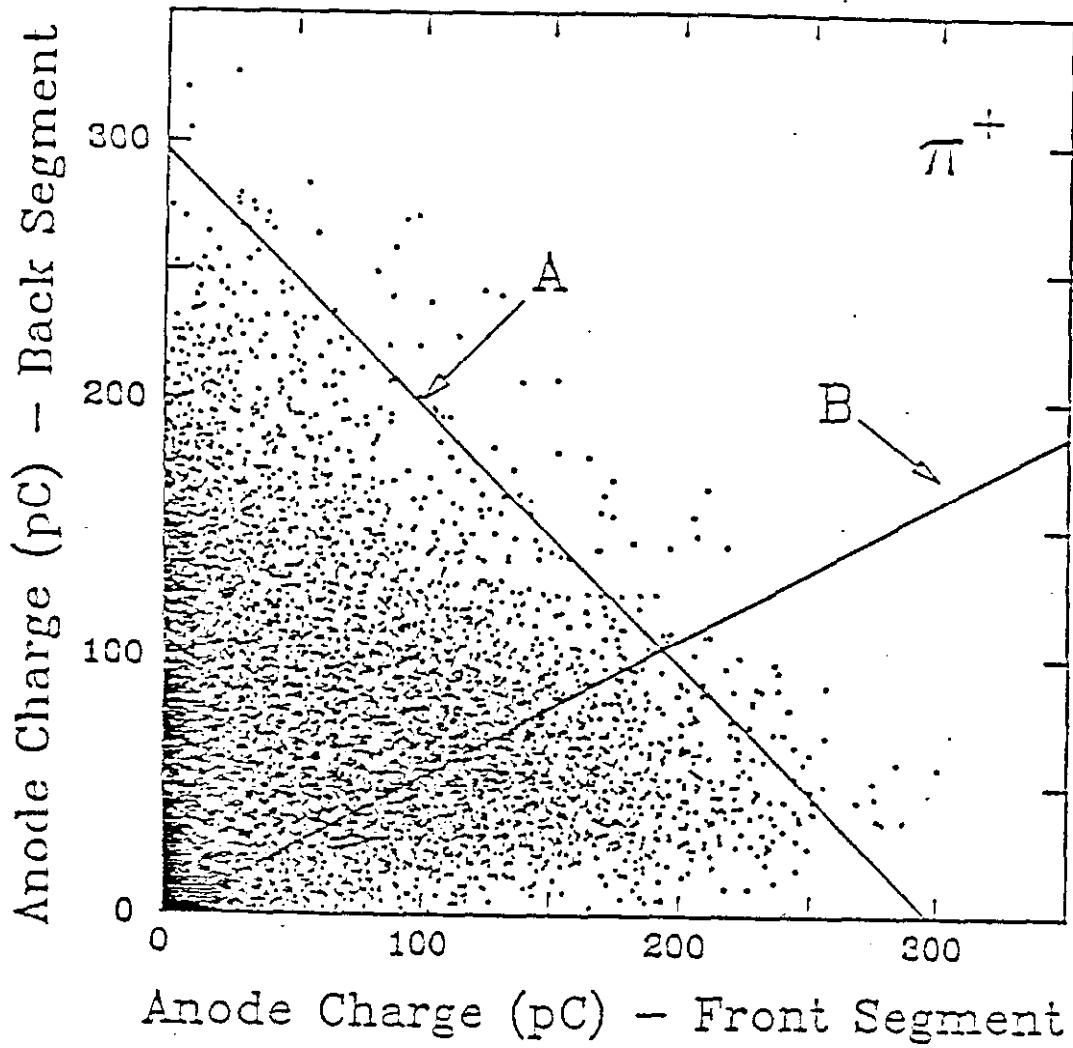


Figure 26: Energy in front half of electromagnetic calorimeter versus energy in back half for 60 GeV pions. Solid lines correspond to cuts A and B as discussed in the text. Events surviving both cuts are to the right of line A and below line B respectively.

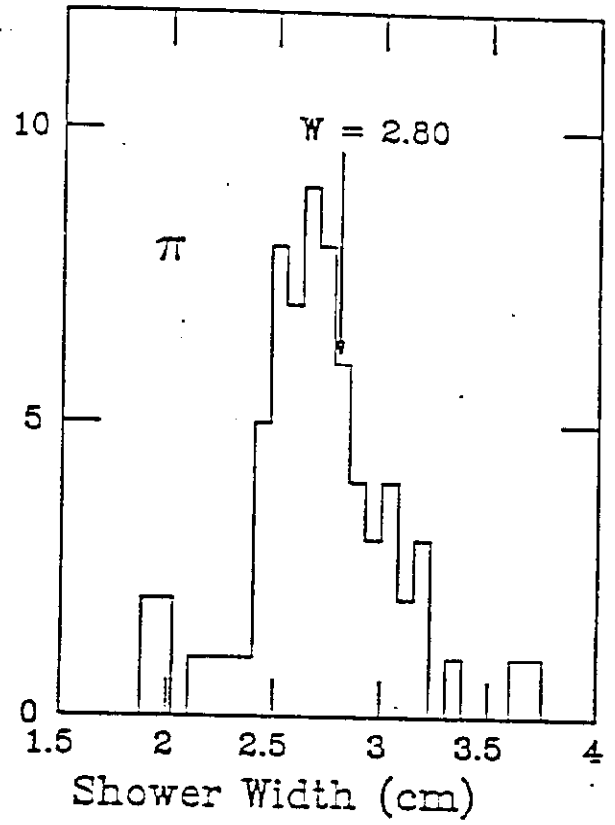
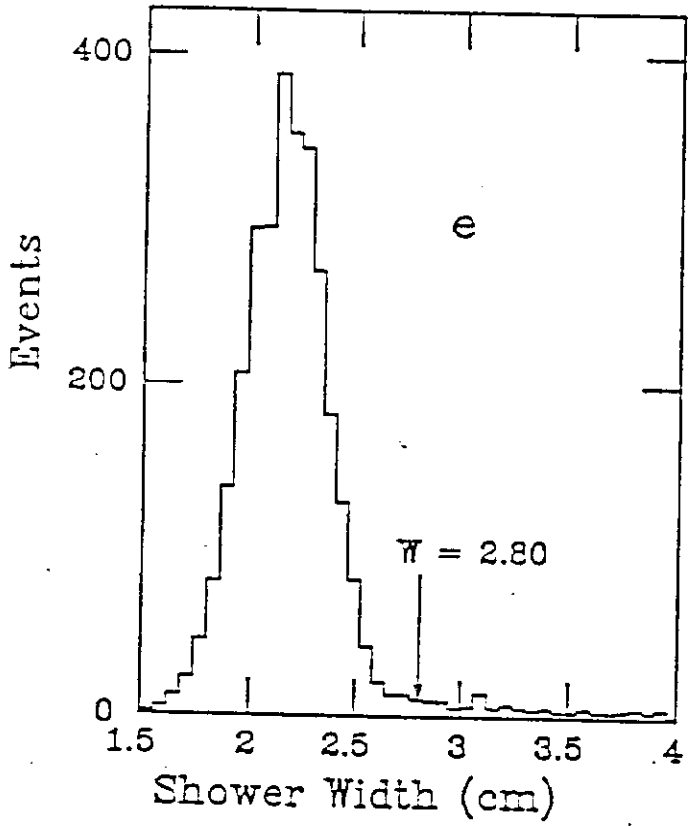


Figure 27: Distribution of shower widths for electrons and pions. The cut C is shown.